Energy-efficient heating strategies of diesel oxidation catalyst for low emissions vehicles

Hamedi, Mohammad Reza; Doustdar, Omid; Tsolakis, Athanasios; Hartland, Jonathan

DOI:
10.1016/j.energy.2021.120819

Document Version
Peer reviewed version

Citation for published version (Harvard):
Hamedi, MR, Doustdar, O, Tsolakis, A & Hartland, J 2021, 'Energy-efficient heating strategies of diesel oxidation catalyst for low emissions vehicles', *Energy*, vol. 230, 120819. https://doi.org/10.1016/j.energy.2021.120819

Energy-efficient heating strategies of diesel oxidation catalyst for low emissions vehicles

Mohammad Reza Hamedi[1], Omid Doustdar[1], Athanasios Tsolakis[1,*], Jonathan Hartland[2]

Abstract

Electrically heated catalyst (EHC) is integrated with the exhaust aftertreatment system to reduce cold-start emissions. Implementation of this proposed emission control technology will also provide addition CO_2 and fuel consumption benefits. Developing an energy-efficient heating strategy has shown a significant reduction in the time required for the catalysts to light-off from the cold-start. In this study, it was found for the first time that the novel pulsating heating strategy with the pulse width of 30 seconds compared with typical heating strategy improved the CO and THC emissions conversion efficiency up to 34% and 31%, respectively. In contrast, a further increase in the heating pulse leads to lower emissions' conversion performance due to extending heating off period and consequently leading to the catalyst's light-out. Furthermore, combined electrical and fuel post-injection catalyst heating can benefit from the EHC's quick catalyst light-off and higher heating efficiency of the fuel post-injection, which showed a significant improvement in the DOC's emissions conversion performance. This approach can result in higher catalyst heating efficiencies and lower THC emissions which can be critical to meet the emissions legislations. An increase in the DOC's outlet temperature can be also beneficial for downstream aftertreatment component heating, e.g. DPF regeneration.

Keywords: Engine cold-start, Thermal management, Aftertreatment, Electrically heated catalyst, Catalyst light-off, Gaseous emissions

[1] Department of Mechanical Engineering, School of Engineering, University of Birmingham, Birmingham B15 2TT, UK

[2] Powertrain Research and Technology, Jaguar Land Rover, Coventry, UK

[*] Corresponding author, E-mail address: a.tsolakis@bham.ac.uk (A.Tsolakis)

Nomenclature

Abbreviations

AC	Alternating current
C_2H_4	Ethylene
C_3H_6	Propylene
CH_2O	Formaldehyde
CH_3CHO	Acetaldehyde
CI	Compression ignition
CO	Carbon monoxide
CO_2	Carbon dioxide
CO_x	Carbon oxides
COV	Coefficient of variation
cpsi	Cells per square inch
DOC	Diesel oxidation catalyst
DPF	Diesel particulate filter
EHC	Electrically heated catalyst
FTIR	Fourier transform infrared
GHSV	Gas hourly space velocity
H_2O	Water
HC	Hydrocarbon
HEV	Hybrid electric vehicle
IC	Internal combustion
IMEP	Indicated mean effective pressure
ISFC	Indicated specific fuel consumption
LNT	Lean NO_x trap
Mil	Milli-inch
N_2	Nitrogen
N_2O	Nitrous oxide
NEDC	New European driving cycle
NO	Nitric oxide
NO_2	Nitrogen dioxide
NO_x	Nitrogen oxides
O_2	Oxygen
Pd	Palladium
PCM	Phase change material
P-EHC	Pulsating electrically heated catalyst
PGM	Platinum-group metals
PM	Particulate matter
ppm	Parts per million
Pt	Platinum
PW	Pulse width
Rh	Rhodium
RPM	Revolutions per minute
SCR	Selective catalytic reduction
SI	Spark ignition
TDC	Top dead centre
THC	Total hydrocarbons
TWC	Three-way catalyst
ULSD	Ultra-low sulphur diesel

Notations

A	Reaction pre-exponential factor
C_p	Specific heat capacity ($J/kg^{-1}.K^{-1}$)
D_c	Catalyst diameter
D_p	Pipe diameter
E_a	Reaction activation energy ($J.mol^{-1}$)
G	Inhibition term
h	Sensible enthalpy ($J.kg^{-1}$)
H	Enthalpy ($J.kg^{-1}$)
h_c	Convective heat transfer coefficient ($W.m^2.K$)
k	Reaction rate constant
k_j	Mass transfer coefficient species j ($m.s^{-1}$)
L_c	Catalyst length
L_p	Pipe length
r	Radial dimension
R	Reaction rate ($mol.m^3.s^{-1}$)
RT	Universal gas constant
S	Heat source term ($W.m^{-3}$)
S_F	Shape factor for heat conduction
t	Time(s)
T	Temperature (K)
v	Velocity ($m.s^{-1}$)
V	Volume (m^3)
v_f	Volume fraction
y_j	Molar fraction of species j
z	Axial dimension
β	Liquid fraction
ε	Void fraction of the monolith
ε_{rad}	Emissivity factor
λ	Thermal conductivity ($W.m^{-1}.k^{-1}$)
ρ	Density ($kg.m^3$)
σ	Stefan-Boltzmann constant ($W.m^{-2}.K^4$)

Subscripts

amb	Ambient
g	Exhaust gas
j	Component of exhaust gas
s	Solid

1. Introduction

Many European governments are now scheduling the phasing-out of conventional diesel and gasoline vehicles, and yet it will be several decades before most road vehicles are fully electrically powered [1]. The impact of emissions from conventional road vehicles on the environment and human health has led to the introduction of stringent emissions legislation, such as EUROs in the European Union [2]. Some emission control technologies still have significant limitations in economic viability and global warming concerns [3], which in the short term lead to having solutions with better combustion, aftertreatment systems [4] and in the medium term with the development of new alternative fuel and advanced engine systems [5]. Also, catalytic emission control technologies are more straightforward and do not require modifying the engine since they are only focused on reducing the light-off temperature and time, particularly during engine cold-start and warm-up. In recent years, to reduce compression ignition (CI) engines emissions, different aftertreatment technologies such as diesel oxidation catalysts (DOC) [6], selective catalytic reduction (SCR) [7], lean NO_x traps (LNT) [8], and diesel particulate filter (DPF) [9] have been used. These aftertreatment systems reduce the required activation energy for emissions' conversion reactions to oxidise carbon monoxide (CO), hydrocarbons (HC) and particulate matter (PM) and nitrogen oxides (NO_x) reduction [10].

It is crucial to achieving the highest performance of the aftertreatment system at the lowest temperature and as soon as possible. During engine cold-start and warm-up, the functionality of these catalytic converters deteriorate due to low temperature [11], and the engine consumes more fuel than normal conditions in order to reach the aftertreatment system catalyst activation temperature [12]. Up to 80% of CO and HC emissions are emitted during the cold-start period [13]. As an example, hybrid electric vehicles (HEV) engines are usually off at low speed, when the brake specific fuel consumption is high, this reduces exhaust temperature and thus catalytic converters performance [14]. Different thermal management technologies have been proposed to overcome this issue, including retarded fuel ignition timing, increased idle engine speed, lean

air/fuel ratio operation [15], chemically design modification of catalysts [12], electrically heated catalysts (EHC) [13], exhaust system combustion devices, secondary air injection into the exhaust, preheating engine strategies [16], phase change materials (PCM) [17], advanced combustion strategies [18] and alternative fuels combustion [19].

Among these technologies, EHC allows direct delivery of thermal energy from the vehicle's battery or onboard generator into the aftertreatment system when required. This technology can quickly improve the catalytic converter performance in the control of cold-start CO and THC emissions from hybrid vehicles [20]. This application can also preheat the catalyst (while the vehicle is running on a battery with off engine) for quick catalyst light-off after the engine is turned on [20]. Trends in vehicles hybridisation and electrification make the application of EHC a promising alternative method to other engine-based catalyst heating strategies for future vehicles [21]. The main advantages of an EHC compared to engine-based heating strategies are: i) direct application of thermal energy at the catalyst site [22], ii) the higher degree of control over the heating intensity and period [23], iii) reduced loading of precious metals for catalysts [24] and iv) potential in reducing vehicles' carbon dioxide (CO_2) emissions, as the engine can be recalibrated to more efficient conditions [21]. Knorr et al. [25] found the potential HC, CO, NO_x and CO_2 exhaust emission reduction and lower fuel consumption for HEV equipped with EHC coupled with advanced aftertreatment system compared with conventional engine-based catalytic convertor heating strategies. Pace et al. [26] also indicated that the use of EHC to provide thermal energy to increase the catalyst temperature is only 40% of the energy of the additional injected fuel to achieve the same effect based on the engine parameter method. Horng et al. [27] found that the light-off time with an EHC was less than 180 seconds, shorter than the fuel enrichment method.

Socha et al. [28] studied various EHC configurations for an SI engine's three-way catalytic (TWC) converter. In order to further decrease the heater's electrical energy consumption, the heater's mass was reduced to decrease the system's thermal inertia. The electrical heating of the

catalyst before the engine's start was also examined and found to be more efficient in reducing emissions compared to heating during the cold-start. Massaguer et al. [29] propose the use of a thermoelectric generator coupled to an exhaust gas heat in SI engines TWC system. Their system could reduce up to 94%, 91% and 97% of the pollutant emissions for NO_x, HC and CO, respectively. Similarly, Zobel et al. [30] proved the significant improvement in cold-start emissions reduction up to 91% with the combined effect of spark advance, air/fuel ratio and EHC in a power plant that uses natural gas-fuelled IC engines as a power generator and TWC as aftertreatment system.

In work by Pfahl et al. [24], a heating disk with an electrical power of 1 kW was positioned upstream the DOC of a 3 L diesel engine. The heater was turned on for the first 100 seconds of the New European Driving Cycle (NEDC), and the DOC light-off was achieved approximately 100 seconds earlier, compared to the reference case without electrical heating. This resulted in a 60% and a 25% reduction in CO and HC emissions over the NEDC, respectively. To reduce NOx emissions, a 1.9 kW heater was used upstream of an SCR to improve urea solution evaporation, decomposition and hydrolysis. Approximately a 40% reduction in NO_x emissions was achieved with the extended heating period [24]. Gao et al. [31] also investigated the influence of different EHC control strategies in diesel engine evaluated based on emission reduction and energy consumption. The use of EHC in their aftertreatment system leads to a significant reduction of cold-start CO and HC emissions by at least 50%.

Furthermore, Kim et al. [32] investigated the effect of an EHC with 8.3 kW of electrical power upstream of DOC and SCR for a medium-duty 6.6 L diesel engine. Fuel injection was also used to improve the SCR emissions conversion performance after the DOC's temperature reached 250 °C with electrical heating assistance. High-intensity electrical catalyst heating was proved to be considerably more efficient compared to electrical heating with lower power and a longer heating period. Fuel injection was also found to be beneficial to reduce the NO_x emissions when the DOC's temperature was higher than 250 °C, as the tested DOC was able to oxidise most of the injected hydrocarbons above this temperature level [32].

Fuel post-injection is widely used for DPF regeneration due to an increase in the exhaust gas temperature, while it increases the unburnt hydrocarbons and CO emissions which can be oxidised over the DOC [14]. Post injection is also used to provide hydrocarbons for lean NO_x traps to regenerate the stored NO_x [33]. Three main theories are behind the underlying mechanism. Firstly, post-injection increases the combustion chamber's temperature during the late phases of combustion [34], which can assist soot oxidation [35]. Secondly, several studies have discussed that post-injection can enhance in-cylinder mixing, affecting soot formation and oxidation [36]. Finally, a few studies have related the soot formation to the main injection duration [37]. Since the main injection duration can often be reduced by applying post-injection, this can explain a decrease in the engine's PM emissions, particularly for early post-injection [38]. A few studies have also found that post-injection can decrease diesel engine's NO_x emissions by reducing the maximum in-cylinder temperature, as some of the fuel is burned later in the cycle [39]. However, introducing post-injection generally reduces the engine's thermal efficiency and consequently increases the vehicle's fuel consumption [40].

Yamamoto et al. [41] investigated hydrocarbon speciation of a diesel engine's exhaust gas with post-injection at different timings. It was found that the post injected long-chain hydrocarbons are thermally decomposed into smaller hydrocarbons. This resulted in a higher concentration of some alkenes (e.g. C_2H_4 and C_3H_6), formaldehyde (CH_2O), acetaldehyde (CH_3CHO) and CO in the exhaust gas composition with post-injection. Retarding the post-injection timing showed an increase in the gas phase concentration of larger hydrocarbon species (e.g. C_{13} – C_{17}) in the exhaust gas. This can be associated with lower thermal decomposition and oxidation of the hydrocarbons as the temperature of the combustion chamber decreases during the late phases of the expansion stroke [41].

This research work aims to develop an efficient diesel aftertreatment active heating strategy applicable in HEV to reduce vehicles' tailpipe emissions. Also, synergies between electrical heating and fuel post-injection strategies were investigated in order to provide additional energy

to the catalyst for maximising its emissions' conversion performance and reduce fuel consumption. These original energy-efficient heating strategies can be implemented in all catalytic converter systems to meet stringent emissions legislation, particularly for cold-start application. Also, a novel pulsating technology method is developed to enhance the oxidation reaction of CO and THC. This investigation enriches the research with HEV on the moving towards low-emission vehicles. For the experiment, an engine testbed facility was used to evaluate the effectiveness of these heating methods. At the same time, Exithermia Axisuite® aftertreatment modelling was carried out to provide more insight into the underlying physical and chemical phenomena, particularly during a driving cycle.

2. Modelling and Experimental Methodology

In the present study, aftertreatment simulation and experimental investigation have been carried out. Initially, in the Exithermia Axisuite®, timing and position of the electrical catalyst heating were studied. Finally, experimental work is carried out in a single-cylinder diesel engine to investigate different energy-efficient strategies to improve the aftertreatment performance.

2.1. Exothermia Axisuite® Aftertreatment Modelling

In the present study, to have more fundamental insight into the underlying physical and chemical aspects, the aftertreatment simulation was carried out in the commercial Exothermia Axisuite® package. This software is able to model the transient behaviour of aftertreatment components, including flow-through catalysts and predict their time-based temperature profiles and exhaust gas composition [10]. To investigate the thermal behaviour of the DOC, a model was developed and validated based on a standard Axisuite DOC model and experimental data from Euro 5 V6 Jaguar Land Rover diesel engine. Detailed model characteristics and assumptions are presented in [42].

2.1.1. Model Geometry and Boundary Conditions

The model's geometry was created based on a close-coupled full-size DOC substrate, as illustrated in Figure 1. The Pt/Pd based DOC was modelled as a heterogeneous ceramic catalyst with a cell density of 400 cpsi, a wall thickness of 4 Mil, and a volume of 3 L. An upstream pipe that connects the turbocharger to the catalyst was also considered in this model. The geometry was discretised as an axisymmetric 2D structured grid. To simulate a low-load engine condition, the NEDC shown in Figure 2 was selected with an emphasis on its urban part (0-800s). The exhaust gas composition, mass flow rate and temperature profile at the system inlet were extracted from a Euro 5 V6 Jaguar Land Rover diesel engine, as shown in Figure 2. Ambient temperature and pressure were assumed to be 25 °C and 101 kPa, respectively.

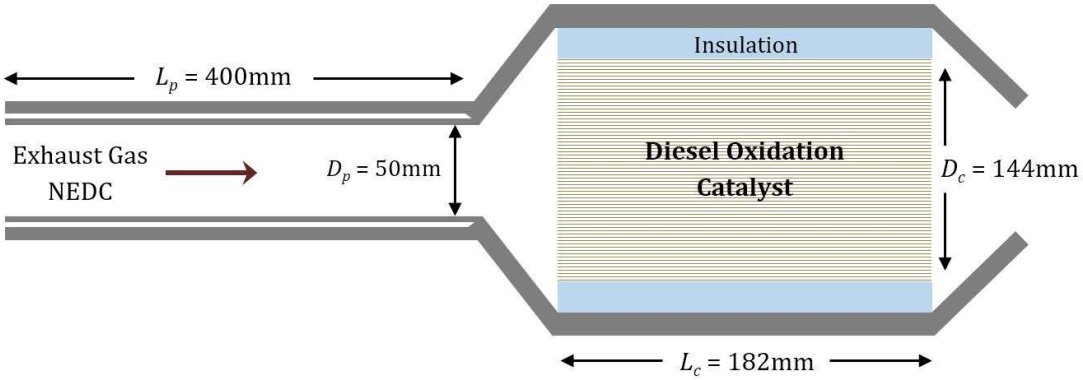

Figure 1: Axisuite® Aftertreatment Model Geometry Diagram

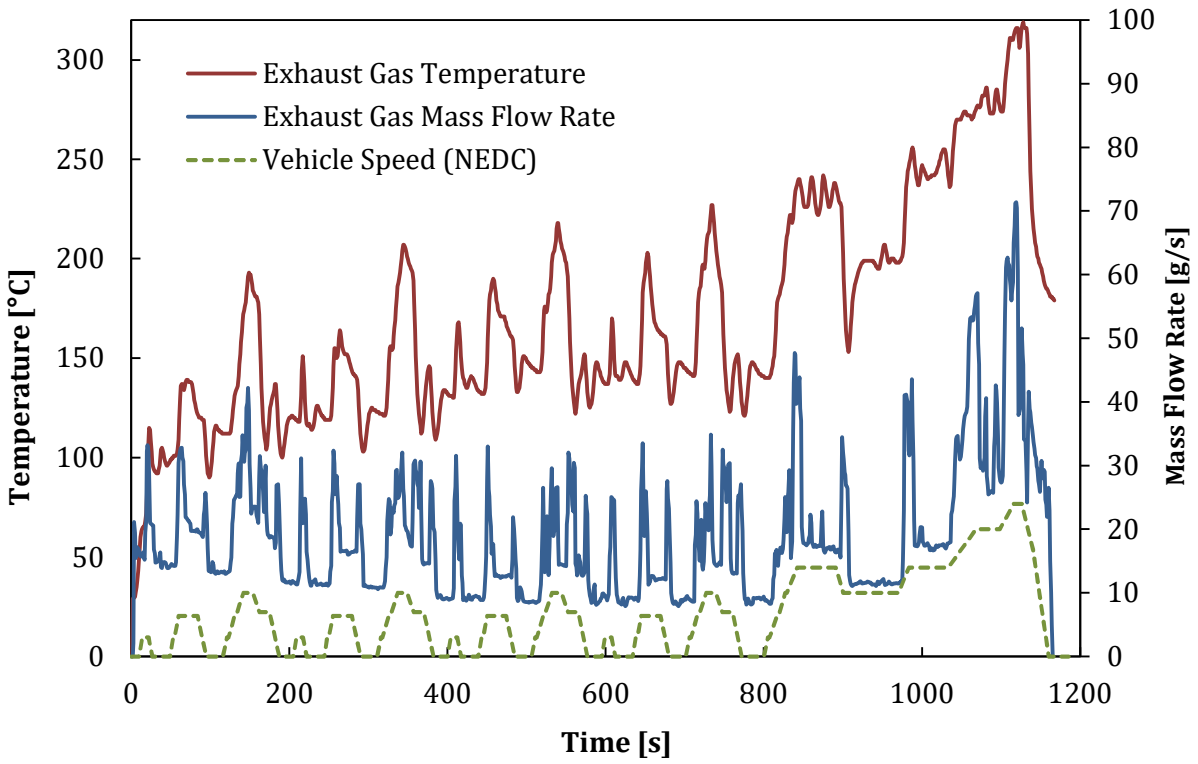

Figure 2: Exhaust Gas Temperature and Mass Flow Rate at the System Inlet

2.1.2. Modelling Theory and Governing Equations

The simulation is fundamentally based on the conservation of mass, momentum, energy and species in solid and fluid parts. Since the exhaust gas pressure variation in the aftertreatment system lies in the order of a few millibars, the flow was assumed incompressible, and the exhaust gas density was determined as a function of the temperature. The Axisuite software assumes a quasi-steady state, as the characteristics time (1 second) is considerably higher than the flow residence time. Heat transfer phenomenon, including conduction, convection within the near-wall region and radiation in the upstream pipework, were considered as shown in Figure 3.

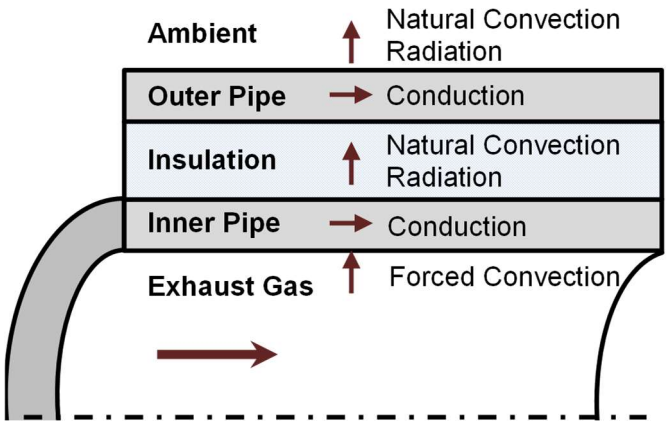

Figure 3: Exhaust Pipe Heat Transfer Modes

The energy balance of the catalyst's solid phase was described by the heat conduction equation in polar coordinates as follows:

$$\rho_S . C_{p,S} \frac{\partial T_S}{\partial t} = \lambda_{S,z} \frac{\partial^2 T_S}{\partial z^2} + \lambda_{S,r} \frac{1}{r} \frac{\partial}{\partial r} \left(r \frac{\partial T_S}{\partial r} \right) + S \qquad \textbf{Equation 1}$$

The heat source term (S) includes the convective and radiative heat transfer of the exhaust gas in the catalyst channels, the heat released or adsorbed by chemical reactions and heat supplied by a heating device where applicable. The heat balance in the catalyst was solved by an implicit finite volume method.

The catalyst's periphery heat losses to the atmosphere by free convection, forced convection and radiation are taken into account as boundary conditions:

$$\lambda_{S,r} \frac{\partial T_S}{\partial r} = C_{amb} \cdot h_{c,amb} (T_S - T_{amb}) + \varepsilon_{rad} \cdot \sigma \cdot \left(T_s^4 - T_{amb}^4 \right) \qquad \textbf{Equation 2}$$

The exhaust gas energy balance was used to compute the gas temperature distribution by the following equation:

$$\rho_g C_{p,g} v_g \frac{\partial T_g}{\partial z} = -h_c \cdot \frac{S_F}{\varepsilon} \cdot \left(T_g - T_S\right) + S_{reaction} \qquad \textbf{Equation 3}$$

The mass balance of gas species j was used to compute the species' concentration distribution along the catalyst's channel as follows:

$$\frac{\partial (v_g y_{g,j})}{\partial z} = -k_j \cdot \left(\frac{S_F}{\varepsilon}\right) \cdot \left(y_{g,j} - y_{S,j}\right) \qquad \textbf{Equation 4}$$

where ρ is density, C_p is specific heat capacity, T is temperature, t is time, λ is thermal conductivity, r is radial dimension, z is axial dimension, h_c is convective heat transfer coefficient, ε_{rad} emissivity factor, σ is Stefan-Boltzmann constant, S_F is shape factor for heat conduction, v is velocity, y_j is molar fraction of species, k_j is mass transfer coefficient of species, ε is void fraction of the monolith. *s* , *g* and *amb* stand for solid, gas and ambient, respectively. The underlying model solver offers the possibility of calculating the coupled transport and reaction phenomena in flow-through catalysts. The chemical reaction rates on catalyst active sites were calculated using the Langmuir-Hinshelwood theory and global reaction rate expressions [43]. The rate of chemical species adsorption on the catalyst surface was also calculated using the Dubinin-Radushkevic equilibrium isotherm and appropriate kinetic rates [44]. The reaction scheme includes CO and hydrocarbon species oxidation with O_2 and NO_2, while NO reversible oxidation to NO_2 was also included. Considering the oxidation of CO by O_2 as an example (Equation 5), the Langmuir-Hinshelwood theory can describe the rate of reaction (R) as follows:

$$CO + \frac{1}{2} O_2 \rightarrow CO_2 \qquad \textbf{Equation 5}$$

$$R = \frac{k[CO][O_2]}{G} \qquad \textbf{Equation 6}$$

where the reaction rate constant k can be calculated by the Arrhenius equation as follows:

$$k = Ae^{\frac{-E_a}{RT}}$$ **Equation 7**

where RT is the universal gas constant. Inhibition term (G), pre-exponential factor (A) and activation energy (E_a) of different reactions were used in this model are based on the experimentally validated data from the literature.

2.1.3. Model Calibration and Validation

The pulsating nature of exhaust gas and swirl flow upstream of the catalyst was neglected in order to reduce the computational time and cost. Due to the simplification, the model (as mentioned in section 2.1.) was calibrated with respect to the experimental data to ensure sufficient consistency at different operating conditions.

The DOC model was validated by comparison with experimental data from a diesel engine equipped with the engine's stop-start technology provided by Jaguar Land Rover. Figure 4a shows the comparison between the catalyst's outlet temperature of the experimental data and predicted simulation results. Cumulative CO and total hydrocarbons (THC) emissions over the NEDC are also illustrated in Figures 4b and 4c, respectively.

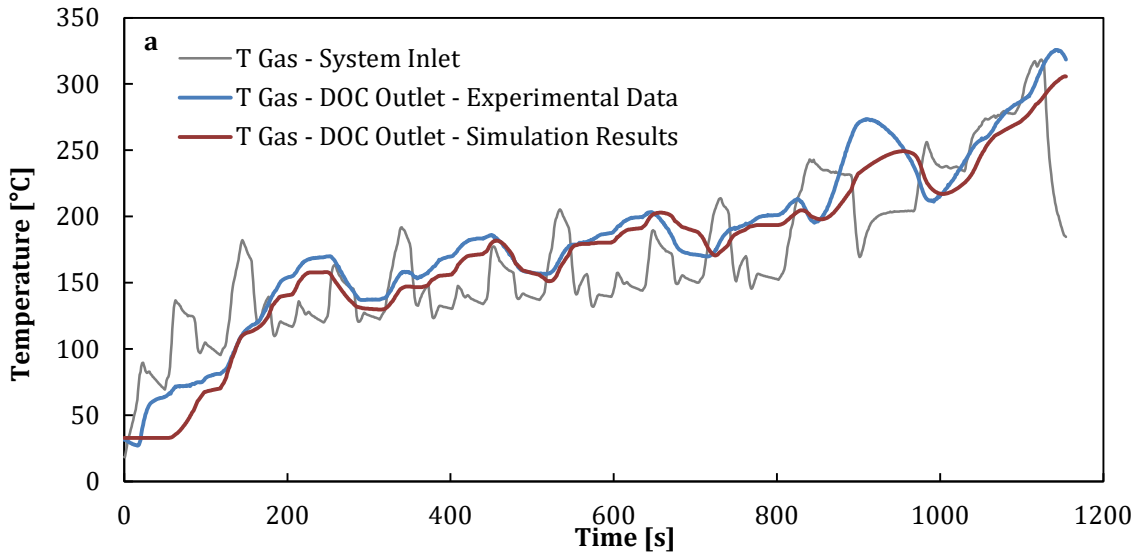
a
T Gas - System Inlet
T Gas - DOC Outlet - Experimental Data
T Gas - DOC Outlet - Simulation Results
Temperature [°C]
Time [s]
0
50
100
150
200
250
300
350
0
200
400
600
800
1000
1200

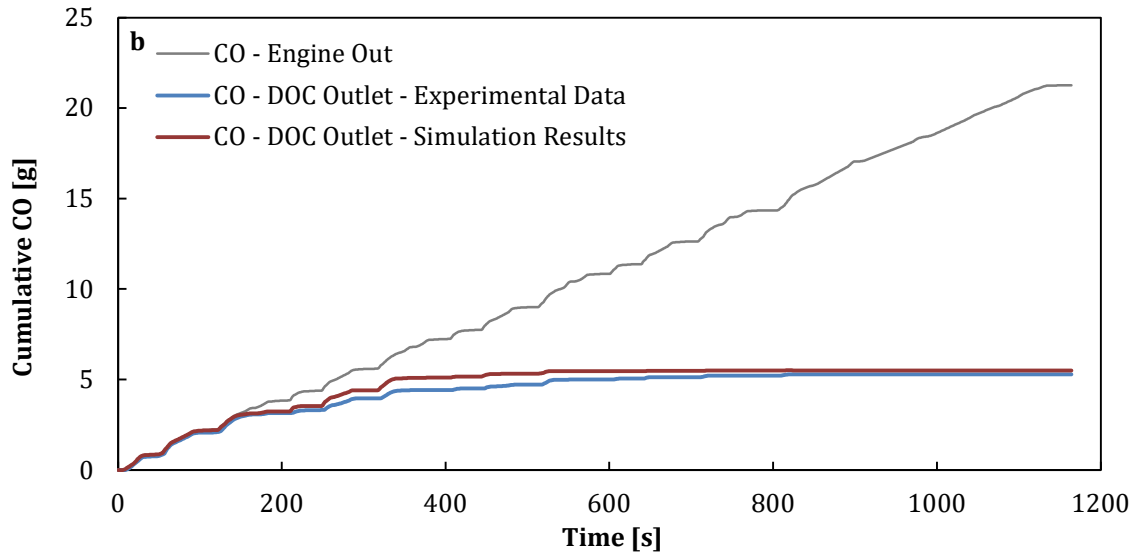
b
CO - Engine Out
CO - DOC Outlet - Experimental Data
CO - DOC Outlet - Simulation Results
Cumulative CO [g]
Time [s]
0
5
10
15
20
25
0
200
400
600
800
1000
1200

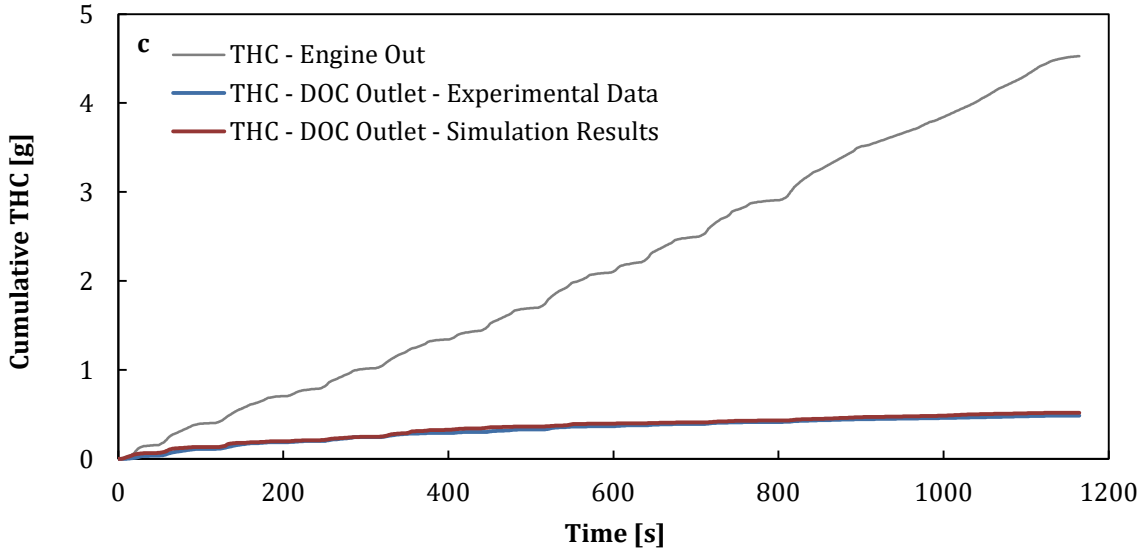
c
THC - Engine Out
THC - DOC Outlet - Experimental Data
THC - DOC Outlet - Simulation Results
Cumulative THC [g]
Time [s]
0
1
2
3
4
5
0
200
400
600
800
1000
1200

Figure 4: Axisuite® Model Validation – a) Temperature Profiles, b) Cumulative CO Emissions, c) Cumulative THC Emissions

The predicted temperature profile slightly underestimates (<6 °C in average) the DOC's outlet temperature, particularly during the NEDC cold-start, which can be associated to water and HC condensation on the DOC's washcoat and the consequent release of the 'latent heat of condensation'. In the case of the CO and THC emissions, adequate consistency was found in the predicted results. In this paper, computational investigations were carried out by modifying relevant model parameters and boundary conditions and their effects on the catalyst's emissions conversion and temperature profiles were observed.

2.1.4. Electrical Catalyst Heating Position Study

Electrical catalyst heating in three different positions was computationally studied, namely, catalyst skin heating, catalyst substrate heating and upstream exhaust gas heating. In the catalyst skin heating, the electrical heater surrounds the catalyst's external periphery, while in the catalyst substrate heating, uniform electrical heating of the full catalyst substrate was assumed. Upstream exhaust gas heating consists of a metallic heating disk with the catalyst's diameter and thickness of 2 cm, which is located before the catalyst's inlet.

In order to investigate the effect of an electrical heater's position on the aftertreatment performance, 2 kW of electrical heating was applied from 30 seconds to 60 seconds after the NEDC cold-start. Furthermore, to further examine the effect of electrical heating position on the catalyst's thermal behaviour, temperature contours of the catalyst's cross-section were investigated. To isolate the heating effect, steady-state exhaust gas at the system's inlet with a temperature of 100 °C and gas hourly space velocity (GHSV) of 15,000 h^{-1} was assumed.

2.1.5. Electrical Catalyst Heating Timing Study

The timing of electrical catalyst heating was investigated using the Axisuite® aftertreatment model. The model includes an upstream exhaust gas heater as introduced in section 2.1.4. During the first 300 seconds of the NEDC, 2 kW of electrical heating was applied in 30-second intervals. Thus 60 kJ of electrical energy was delivered to the heater in each of the studied cases. The DOC's emissions reduction performance was examined as the main criteria to evaluate the effectiveness of the heating's timing.

2.2. Engine Test Bed and Instrumentation

The single-cylinder diesel engine technical data and specifications are summarised in Table 1. The four-stroke diesel engine is naturally aspirated, water-cooled, EGR equipped and utilised a common rail direct fuel injection. An alternating current (AC) electric dynamometer was used to motor and load the engine. The engine was fuelled with ultra-low sulphur diesel (ULSD) supplied by Shell Global Solutions UK. In-cylinder pressure was recorded using an AVL GH13P pressure transducer mounted in the cylinder head, and an AVL FlexiFEM 2P2 amplifier amplified its signal. The crankshaft position was measured by a digital shaft encoder producing 360 pulses per revolution. The pressure and crankshaft position data were combined to create an in-cylinder pressure trace. The temperature at different points was recorded by using k-type thermocouples and a Pico Technology TC-08 thermocouple data logger. An airflow meter was used to measure the engine intake airflow. The engine operating parameters, including the injection strategy, were monitored and controlled by an in-house developed LabVIEW programme connected to a National Instruments PCI-6023E data acquisition device. The programme calculates the engine's indicated mean effective pressure (IMEP) for each cycle. To ensure combustion stability and minimising cyclic variability, the coefficient of variation (COV) of the IMEP for 100 cycles was monitored and kept below 4% during the testing procedure. The engine's fuel consumption under

steady-state condition was recorded, and its corresponding indicated specific fuel consumption (ISFC) was calculated.

Table 1: Test Engine Specifications

Engine Specification	Data
Number of Cylinders	1
Bore	84 mm
Stroke	90 mm
Connecting Rod Length	160 mm
Displacement Volume	499 cc
Compression Ratio	16.1:1
Maximum Injection Pressure	1500 bar
Emissions Standard	Designed for Euro 5
Rated Maximum Power	40 kW @ 5000 rpm

The engine operating condition of 1200 RPM and 2 bar IMEP was selected as the engine rotational speed and load respectively, to reproduce low-load driving conditions. The common rail fuel injection pressure was set at 550 bar. The pilot fuel injection was set to start at 15° bTDC with a duration of 0.150 ms, whereas the main injection started at 3° bTDC with a duration of 0.446 ms. In the cases with fuel post-injection, it started at either 25°, 40° or 55° aTDC as indicated with the duration of 0.100 ms.

2.2.1. Aftertreatment System and Instrumentation

At the 1200 RPM and 2 bar IMEP engine operating condition, the exhaust flow rate was measured at 241 L/min, which corresponds to the DOC's gas hourly space velocity of 49,900 h^{-1}. As schematically illustrated in Figure 5, the exhaust gas travels from the exhaust manifold and passes through 164 cm of pipework to reach the main reactor. This configuration helps to cool down the exhaust gas considerably and provides a more challenging environment for the emissions' reduction in the aftertreatment system. The sampling lines' temperature was kept at 191 °C to avoid hydrocarbon condensation and nucleation. An MKS MultiGas 2030 Fourier

Transform Infrared (FTIR) spectroscopy analyser was used for the analysis of the engine's gaseous emissions, including carbon dioxides (CO_x), nitrogen oxides (NO_x), hydrocarbons (HCs) and water (H_2O). Furthermore, all the measurements were repeated at least three times, and the averaged results are presented.

The exhaust aftertreatment system consists of an electrically heated catalyst (EHC) and a diesel oxidation catalyst (DOC). The size of the aftertreatment reactor was selected to maintain comparable gas hourly space velocity (GHSV) to commercial multi-cylinder engines exhaust aftertreatment systems. The DOC was purchased from Johnson Matthey PLC with the dimensions of 58 mm in diameter and 101 mm in length. The ceramic catalyst substrate was made of cordierite with the cell density of 600 cpsi and a wall thickness of 3 Mil. The catalyst was coated with the platinum group metals' (PGM) loading of 100 g/ft^3 and formulation ratio of 2:1:0 for platinum, palladium and rhodium, respectively. Zeolite was also incorporated into the catalyst coating for improved low-temperature hydrocarbon adsorption and oxidation. Continental Emitec GmbH provided the EHC with the dimensions of 63 mm in diameter and 60 mm in length. It is made of a metallic substrate with 130 cpsi cell density and a wall thickness of 2 Mil. The heating element has a resistance of 0.08 Ω with a maximum operating voltage of 12 V. In this study, the EHC was catalytically uncoated, and it was mainly used as an exhaust gas heater to investigate the heating effect individually. The heating element of the EHC consists of an S-shaped metallic foil matrix that converts electrical energy into thermal energy through electrical resistive means. The EHC was powered using a TDK-Lambda GEN12.5-120 power supply to deliver variable voltage up to 12.5 V, and variable current up to 120 A.

The radial temperature profile at the electrical heater's outlet was investigated to ensure uniformity in the generated heat distribution. Furthermore, the effect of electrical heating power on the DOC's inlet and outlet temperatures was experimentally evaluated. The heating power was adjusted using a variable voltage and current power supply at three different levels (443 W, 603 W and 885 W) considering the requirements for the single-cylinder engine's testbed.

Finally, a new control strategy for the electrically heated catalyst (EHC) was developed and investigated for its effectiveness on the catalyst's emissions reduction performance. This strategy was introduced as pulsating EHC (P-EHC) since the electrical heating power turns on and off with a defined pulse width (PW) over the catalyst's heating period. In this study, the P-EHC's heating efficiency was evaluated based on the DOC's performance when comparing the P-EHC to the EHC with similar electrical energy consumption. Finally, to increase the post-injected fuel catalytic oxidation, a combined catalyst heating approach was investigated.

Moreover, in order to further investigate the pulsating heating effect on the catalyst's behaviour, a computational model was developed in the Axisuite® software based on the experimental specifications and data. For model calibration purposes, the EHC's heating power was assumed to be 4% lower in the model compared to the experimental conditions due to electrical energy losses in the EHC's wiring.

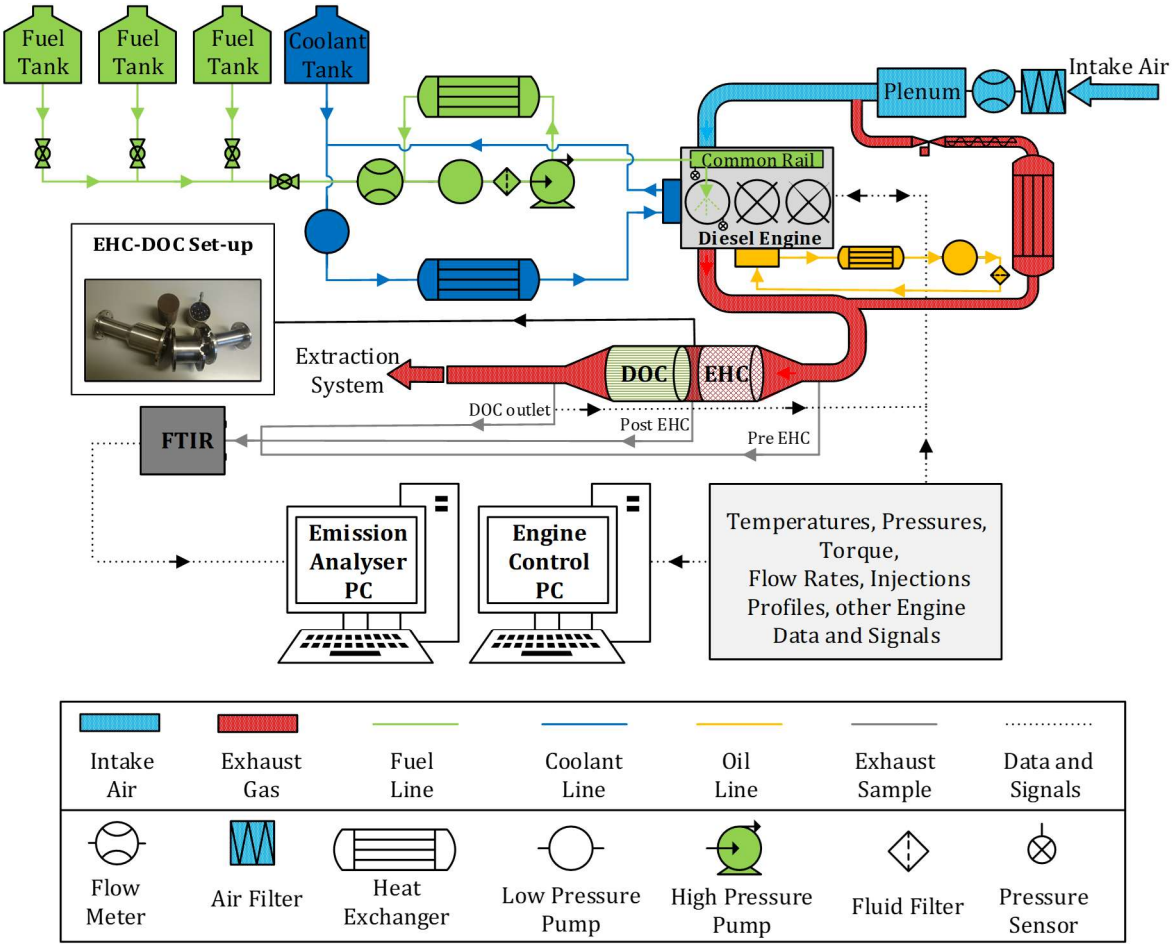

Figure 5: Experimental Set-up Diagram

3. Results and Discussion

3.1. Electrical Catalyst Heating Position Modeling Study

Based on Figure 6a, catalyst substrate heating results in an earlier temperature increase at the DOC outlet due to its relatively closer location to the catalyst's outlet. Upstream exhaust gas heating proved to increase the DOC's outlet temperature by 62 °C at 137 seconds after the cold-start, which is significantly higher compared to the catalyst skin and substrate heating cases. It should be noted that the upstream exhaust gas heating disk increases the aftertreatment thermal inertia, which results in the system's thermal response time being slightly slower. Catalyst skin

and substrate heating can slightly decrease the CO (Figure 6b) and THC (Figure 6c) emissions. However, upstream exhaust gas heating showed a 47% reduction in CO emissions and an 18% reduction in THC emissions compared to the reference case over the NEDC. The CO light-off was achieved at 42 seconds after the cold-start compared to 144 seconds in the reference case. It can be concluded that the significant increase in the upstream heating temperature profile is partially associated with these promoted CO and hydrocarbons exothermic oxidation reactions [45].

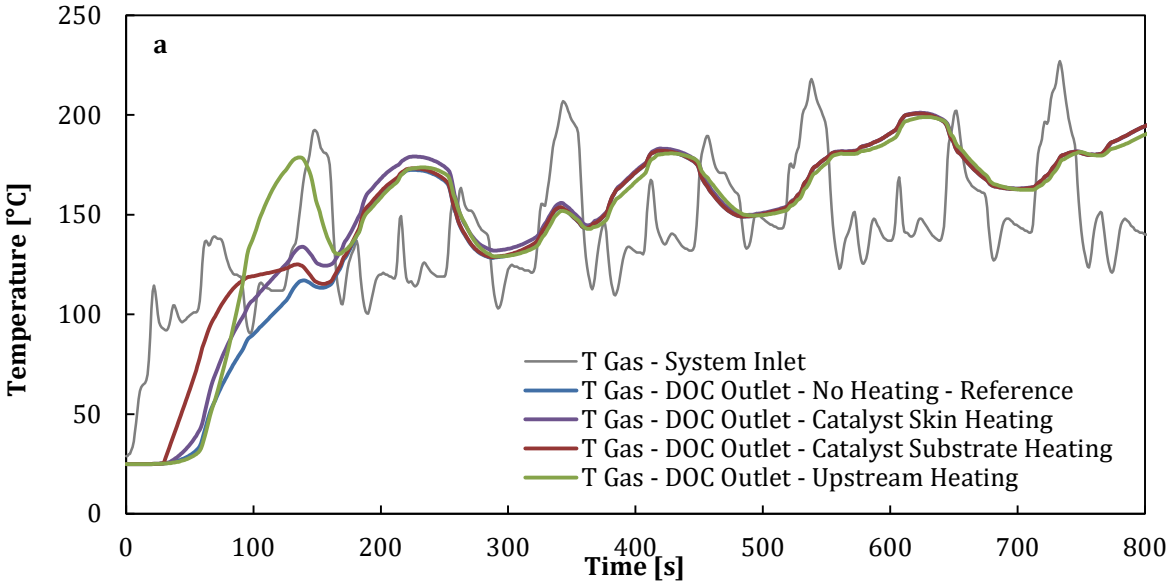
a
Temperature [°C]
Time [s]
T Gas - System Inlet
T Gas - DOC Outlet - No Heating - Reference
T Gas - DOC Outlet - Catalyst Skin Heating
T Gas - DOC Outlet - Catalyst Substrate Heating
T Gas - DOC Outlet - Upstream Heating

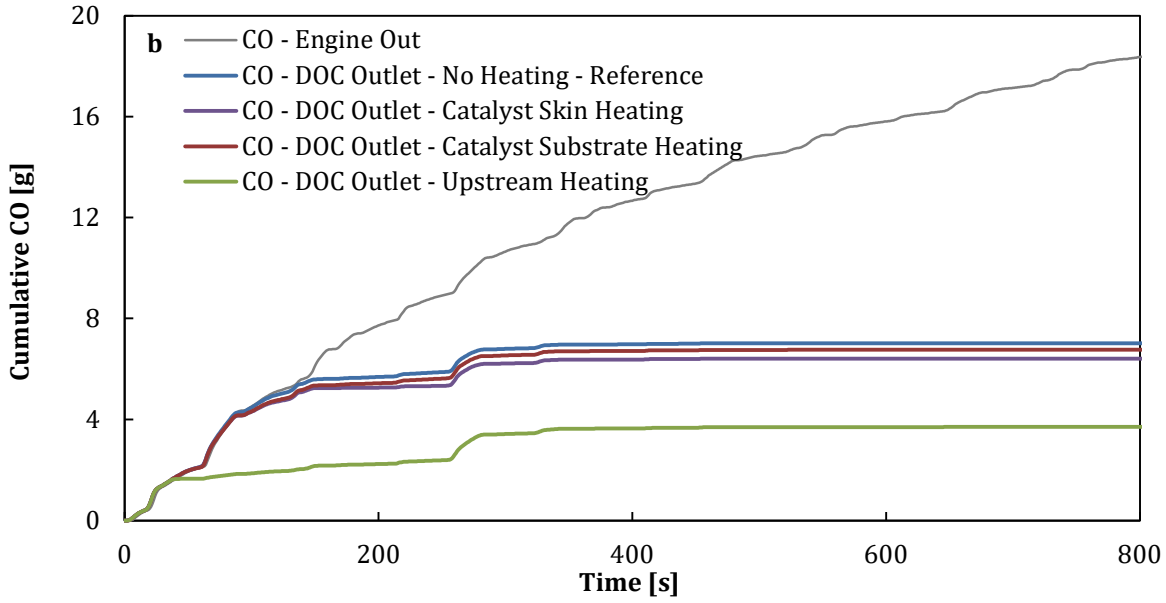
b
Cumulative CO [g]
Time [s]
CO - Engine Out
CO - DOC Outlet - No Heating - Reference
CO - DOC Outlet - Catalyst Skin Heating
CO - DOC Outlet - Catalyst Substrate Heating
CO - DOC Outlet - Upstream Heating

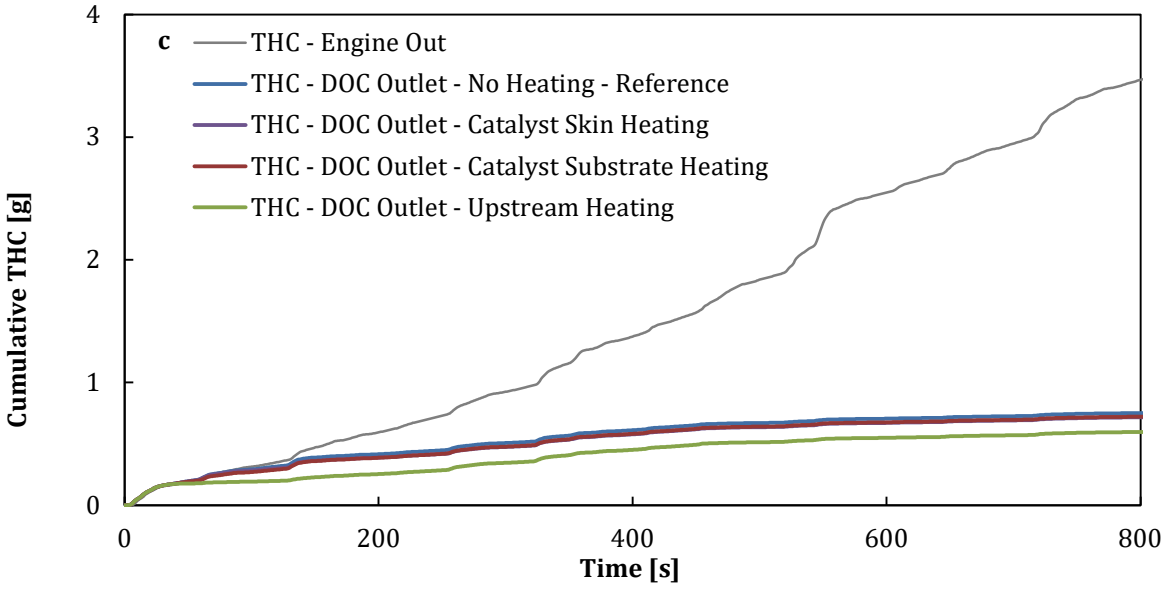
c
Cumulative THC [g]
Time [s]
THC - Engine Out
THC - DOC Outlet - No Heating - Reference
THC - DOC Outlet - Catalyst Skin Heating
THC - DOC Outlet - Catalyst Substrate Heating
THC - DOC Outlet - Upstream Heating

Figure 6: Electrical Catalyst Heating Position Effect on a) the DOC's Temperature Profiles, b) Vehicle's Cumulative CO Emissions, c) Vehicle's Cumulative THC Emissions

Moreover, Figure 7 illustrates the effect of electrical heating position on the catalyst thermal behaviour. Results showed that catalyst skin heating is not able to transfer its heat to the core of the catalyst; this is mainly due to high exhaust gas velocity. Catalyst substrate heating distributes its heat evenly over the substrate's volume. However, the exhaust gas flow tends to transfer this heat towards the catalyst's outlet while passing through the catalyst. In the case of upstream exhaust gas heating, the heater provides concentrated heat at the catalyst's inlet, which can activate the oxidation reactions and form a hot spot that travels through the catalyst after the heating period (Figure 7c). Therefore, this configuration can result in higher DOC emissions' conversion efficiencies and a subsequent increase in the temperature.

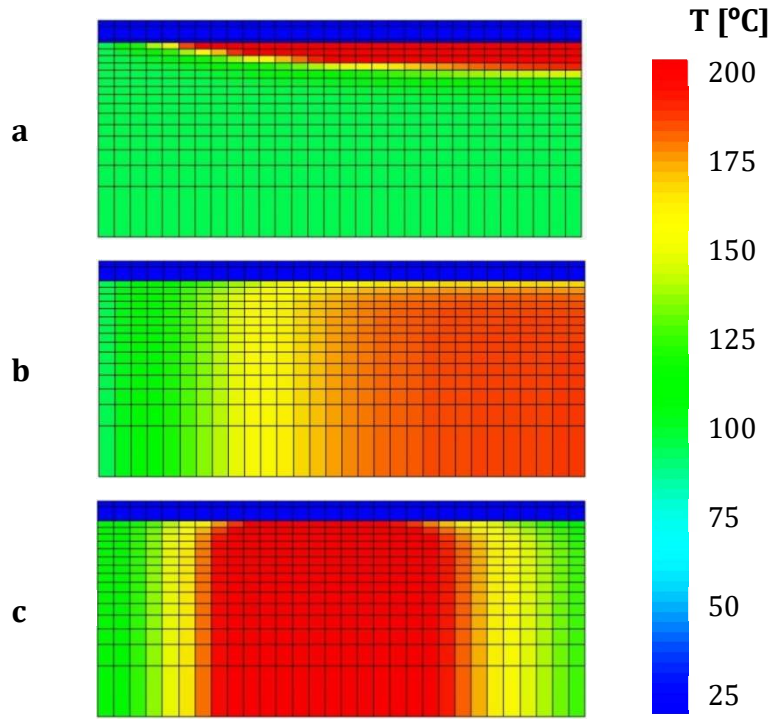

Figure 7: Electrical Catalyst Heating Position Effect on the Catalyst's Temperature Contours: a) Catalyst Skin Heating, b) Catalyst Substrate Heating, c) Upstream Exhaust Gas Heating (10 Seconds after the Heating Period)

3.2. Electrical Catalyst Heating Timing Modeling Study

As listed in Table 2, the 2 kW of electrical catalyst heating during the first 30 seconds of the NEDC, leads to approximately a 28.9% reduction in cumulative CO emissions and a 12.1% reduction in cumulative THC emissions. This is mainly associated with the accelerated DOC's light-off assisted by the electrical heating after the cold-start.

Table 2: Electrical Heating's Timing Effect on the Emissions' Reduction Performance

Heating Timing	Cumulative CO [g]	CO Emissions' Reduction [%]	Cumulative THC [g]	THC Emissions' Reduction [%]
No Heating (Reference)	7.02	-	0.859	-
0 to 30 Seconds	4.99	28.9	0.756	12.1
30 to 60 Seconds	3.71	47.2	0.706	17.8
60 to 90 Seconds	3.79	46.1	0.710	17.4
90 to 120 Seconds	5.86	16.6	0.781	9.1
120 to 150 Seconds	6.39	9.0	0.816	5.1
150 to 180 Seconds	6.19	11.8	0.854	0.7
180 to 210 Seconds	6.06	13.7	0.845	1.6
210 to 240 Seconds	5.99	14.6	0.840	2.2
240 to 270 Seconds	6.17	12.2	0.844	1.8
270 to 300 Seconds	6.86	2.3	0.857	0.3

Among the studied cases, electrical heating during 30 to 60 seconds of the NEDC showed the highest improvement in the emissions' conversion with approximately 47.2% and 17.8% reductions in cumulative CO and THC emissions, respectively. It can be argued that during this period, the provided thermal energy is more able to accelerate the catalyst's light-off and maintain the oxidation reactions since the DOC's inlet exhaust gas temperature has increased considerably. However, electrical heating during the first 30 seconds of the NEDC, initially requires a further increase in the temperature of the relatively colder exhaust gas and catalyst, which can result in decreased heating efficiency. Similarly, during 60 to 90 seconds of the NEDC, the improvement in the emissions' conversion stayed almost the same as the previous interval

that is due to maintaining the oxidation reaction in the DOC after catalyst's light-off. Electrical heating effectiveness gradually decreases for the heating intervals between 60 to 150 seconds of the NEDC; since the inlet exhaust gas temperature rises, which can activate the emissions' reduction reactions without external heating. Following this period, the heating effectiveness tends to improve and reaches its local maximum for the 210 to 240 seconds heating interval. This heating interval can result in approximately a 14.6% improvement in cumulative CO emissions and a 2.2% improvement in cumulative THC emissions.

Figure 8a shows that the DOC's outlet temperature in the reference case decreases to around 129 °C at 290 seconds after the cold-start. This can be attributed to the reduced engine load after the third hill of the NEDC. This temperature drop can light-out the catalyst and considerably increase the emissions, as shown in Figure 8b and 8c. Therefore, electrical heating can be used to assist the catalyst and maintain it activated for the emissions' conversion during this period.

Considering the results, a two-phase electrical heating strategy was investigated in order to accelerate the catalyst's light-off and prevent the catalyst from light-out during the NEDC. This includes 2 kW of electrical heating for 60 seconds (120 kJ of electrical energy) which is divided into two phases. The first phase starts at 20 seconds after the cold-start and lasts for 40 seconds, while the second phase starts at 210 seconds after the cold-start and lasts for 20 seconds. As shown in Figures 8b and 8c, this strategy leads to approximately a 70% reduction in cumulative CO emissions and a 24% reduction in cumulative THC emissions. (For example, the maximum cumulative CO emissions without any heating strategy is 7.02 g, which with heating strategy is reduced to 2.12 g and similarly maximum THC emissions is reduced from 0.86 g to 0.65 g).

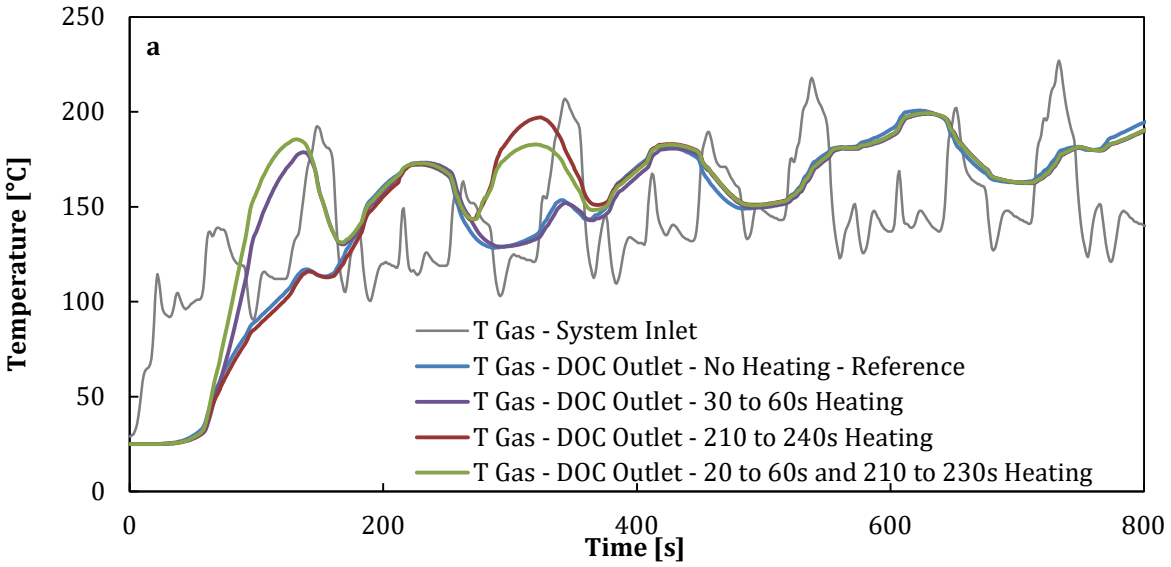
a
Temperature [°C]
250
200
150
100
50
0
0
200
400
600
800
Time [s]
T Gas - System Inlet
T Gas - DOC Outlet - No Heating - Reference
T Gas - DOC Outlet - 30 to 60s Heating
T Gas - DOC Outlet - 210 to 240s Heating
T Gas - DOC Outlet - 20 to 60s and 210 to 230s Heating

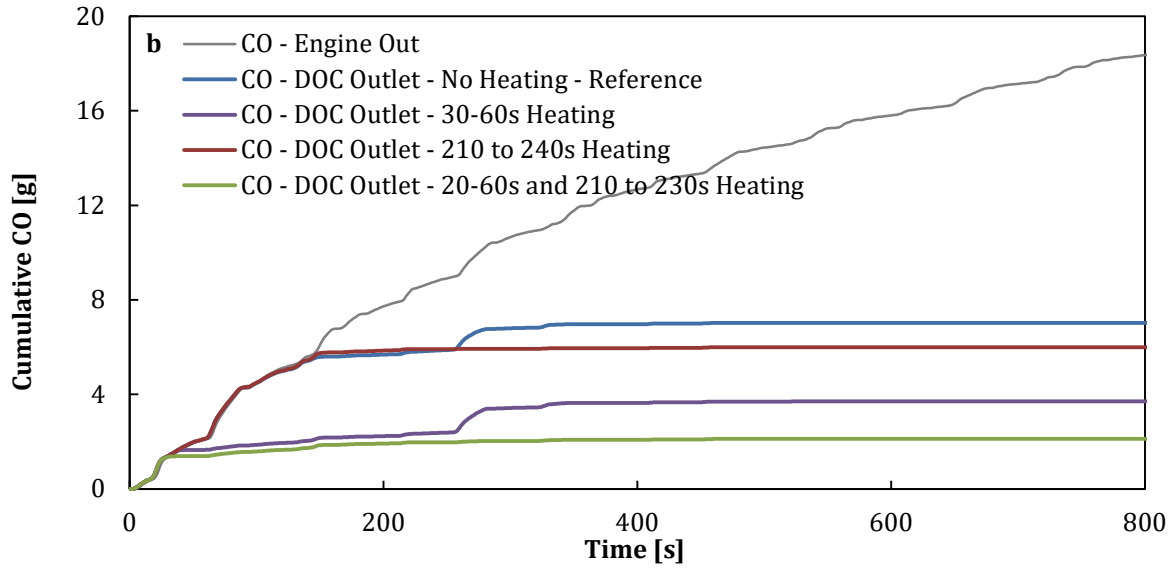
b
Cumulative CO [g]
20
16
12
8
4
0
0
200
400
600
800
Time [s]
CO - Engine Out
CO - DOC Outlet - No Heating - Reference
CO - DOC Outlet - 30-60s Heating
CO - DOC Outlet - 210 to 240s Heating
CO - DOC Outlet - 20-60s and 210 to 230s Heating

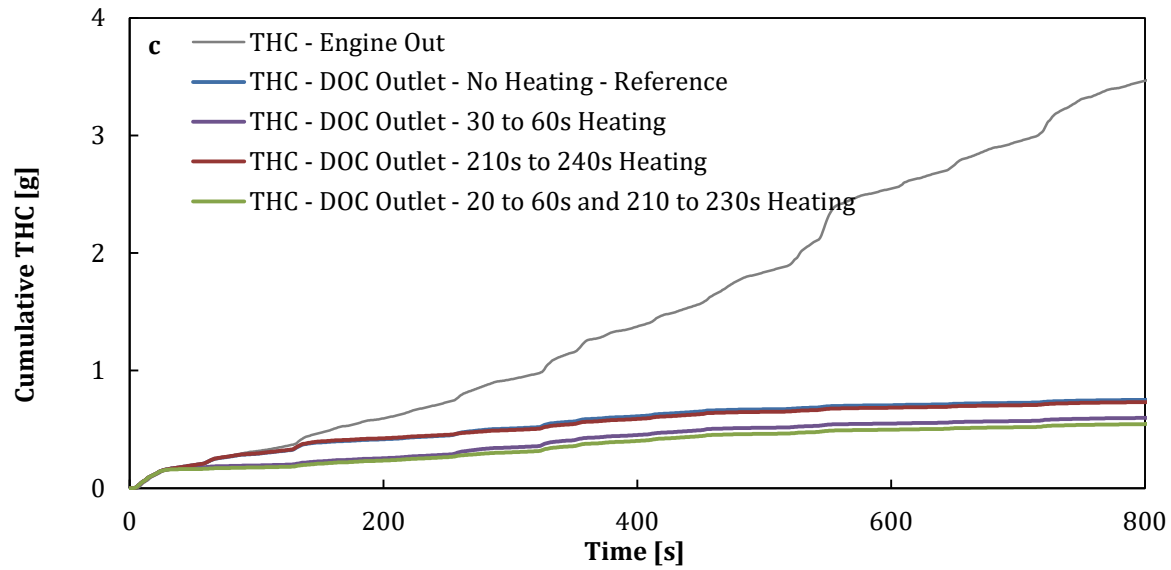
c
Cumulative THC [g]
4
3
2
1
0
0
200
400
600
800
Time [s]
THC - Engine Out
THC - DOC Outlet - No Heating - Reference
THC - DOC Outlet - 30 to 60s Heating
THC - DOC Outlet - 210s to 240s Heating
THC - DOC Outlet - 20 to 60s and 210 to 230s Heating

Figure 8: Electrical Heating Timing Effect on the a) DOC's Temperature Profiles, b) Vehicle's Cumulative CO Emissions, c) Vehicle's Cumulative THC Emissions

3.3. Experimental Steady-State Study of an Electrically Heated Catalyst (EHC)

In the experimental steady-state study of the EHC, the exhaust gas temperature (211 °C) decreases by 79 °C while travelling from the engine's exhaust manifold to the EHC's inlet (132 °C), through a 164 cm length of pipework. A negligible temperature drop (approximately 1 °C) was observed comparing the EHC inlet and outlet temperatures in the reference case with the deactivated off the electrical heater. After the DOC, the exhaust gas' temperature slightly decreases to 128 °C due to the heat loss to the atmosphere in this case. Figure 9 shows that the electrical heater in this study can produce relatively uniform radial temperature profiles at its outlet. This can be beneficial for improving emissions' conversion and minimising the risk of reducing the catalyst's durability.

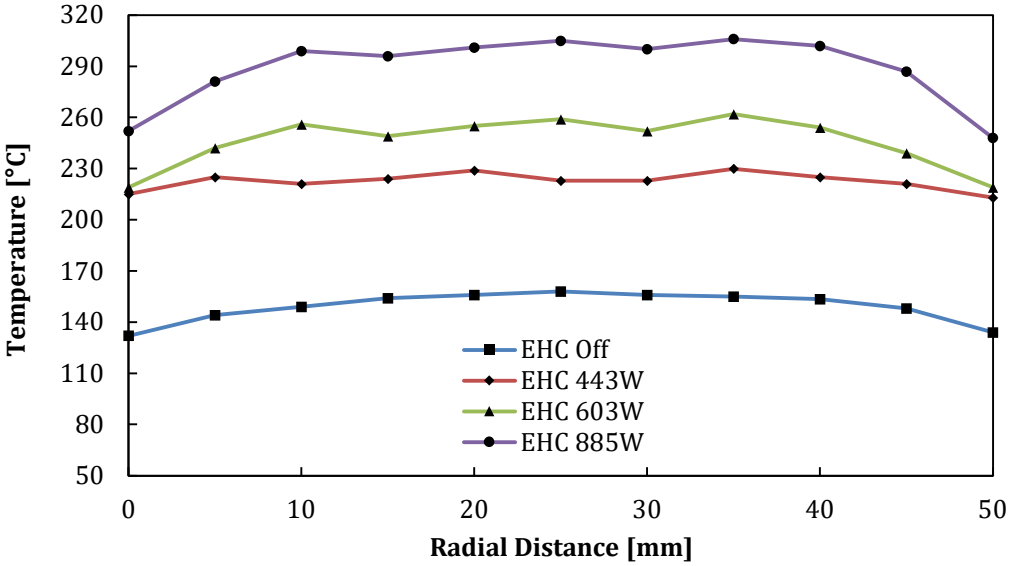

Figure 9: Post Electrical Heater Radial Temperature Profiles at Different EHC Powers

The results of different electrical heating power indicate that 443 W of electrical heating increase the DOC's inlet temperature by 67 °C to 199 °C compared to the reference case (132 °C pre EHC). The 603 W and 885 W of electrical heating increase the DOC inlet temperature to 226 °C and 275 °C, respectively. Also, DOC outlet temperature for 443 W, 603 W and 885 W are 197 °C, 227 °C and 278 °C, respectively.

The reference case when EHC is off in Figure 10 presents that 223 ppm of CO was measured at the DOC's inlet, which decreases to 197 ppm at the DOC's outlet. In the case of the hydrocarbon emissions, 296 and 166 ppm of THC emissions were measured at the DOC's inlet and outlet, respectively. This yields approximately 44% THC conversion efficiency due to hydrocarbons oxidation, adsorption and condensation. It should be noted that the catalyst coating includes zeolite for improved low-temperature hydrocarbon adsorption and oxidation. Moreover, Figure 9 shows that NO emissions' concentrations tend to increase from 241 to 274 ppm while passing through the DOC in the reference case. Simultaneously NO_2 emissions decrease from 47 to 11 ppm, maintaining the total level of NO_x emissions at approximately 287 ppm. It can be concluded that most of the NO_2 was used as an oxidative reactant to promote the CO and THC oxidations in these relatively low-temperature conditions for the DOC.

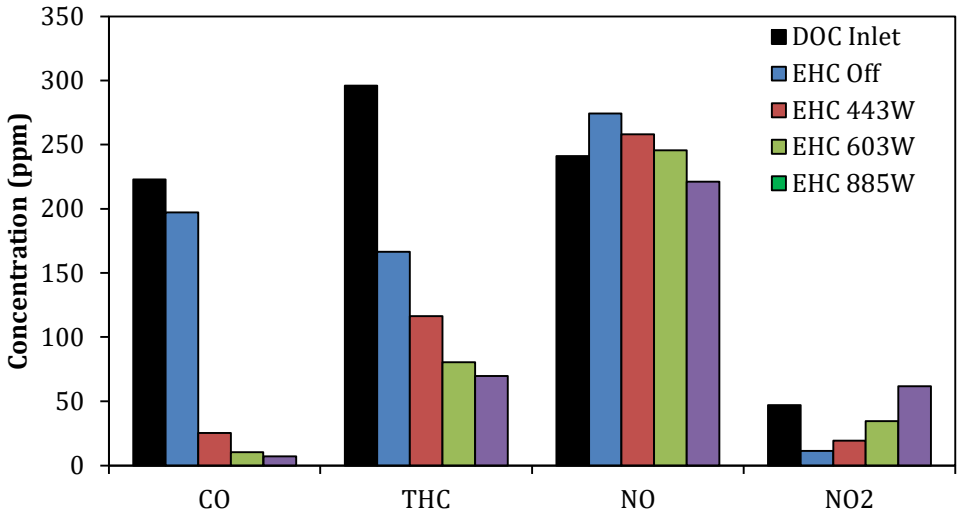

Figure 10: Exhaust Gas Emissions Concentrations in the DOC inlet and The Effect of the EHC's Power on the DOC's Outlet Emissions Concentrations

The conversion efficiency for CO and THC emissions, while EHC is off, are 11% and 44%, respectively. However, 443 W of electrical heating yields approximately 88% and 60% conversion efficiency for the CO and THC emissions, respectively. It can be concluded that the 443 W of electrical heating can provide the required thermal energy to enable the DOC to light-off the CO oxidation reactions in these operating conditions. Although the total NO_x level remains similar, slightly more NO_2 (approximately 19 ppm) was measured in the exhaust gas due to the improved catalyst oxidation activity, which also promoted the NO oxidation to NO_2.

As mentioned above, the DOC's inlet and outlet temperatures were increased to 226 °C and 227 °C, respectively, by 603 W of electrical heating. This results in approximately 95% CO emissions' conversion efficiency and 72% for the THC emissions' conversion efficiency. The exhaust gas' NO_2 concentration was increased to approximately 35 ppm in this case. In the case of 885 W of electrical heating, the DOC's inlet temperature was raised to 275 °C, while the DOC's outlet temperature was increased further to 278 °C due to the promoted exothermic oxidation reactions. This assists the DOC in achieving approximately 97% and 76% conversion efficiencies

for the CO and THC emissions, respectively. Similarly, the NO_2 level was increased to approximately 61 ppm in the DOC's outlet exhaust gas composition in these operating conditions.

3.4. Experimental Study of Pulsating Electrically Heated Catalyst (P-EHC)

The pulsating EHC with a pulse width of 20 seconds (20 seconds on followed by 20 seconds off) and electrical power of 885 W was compared to the EHC at 443 W as shown in Figure 11a. The DOC's inlet temperature (post EHC) tends to fluctuate from 173 °C to 234 °C as the electrical heating turns on and off in the P-EHC case. This results in fluctuations in the DOC's outlet temperature with reduced amplitude (from 199 °C to 212 °C) mainly due to the catalyst's thermal inertia. The average DOC's outlet temperature using the pulsating strategy is approximately 7 °C higher over the heating period compared to the EHC 443W case. Considering that a comparable amount of electrical energy was delivered to the catalyst in both cases, this temperature increase can be explained by promoted exothermic oxidation reactions in the pulsating catalyst heating case.

Based on Figure 11b, CO and THC emissions at the DOC's outlet can be reduced by approximately 18% and 24%, respectively, using the pulsating heating strategy with respect to comparable steady electrical catalyst heating. The results indicated that CO emissions are more sensitive to temperature fluctuations while THC emissions proved to be stable over the pulsating heating period. This can be caused by the hydrocarbon storage capability of the zeolite in the catalyst coating. Figure 11c shows that pulsating heating has a relatively insignificant effect on the NO and NO_2 emissions.

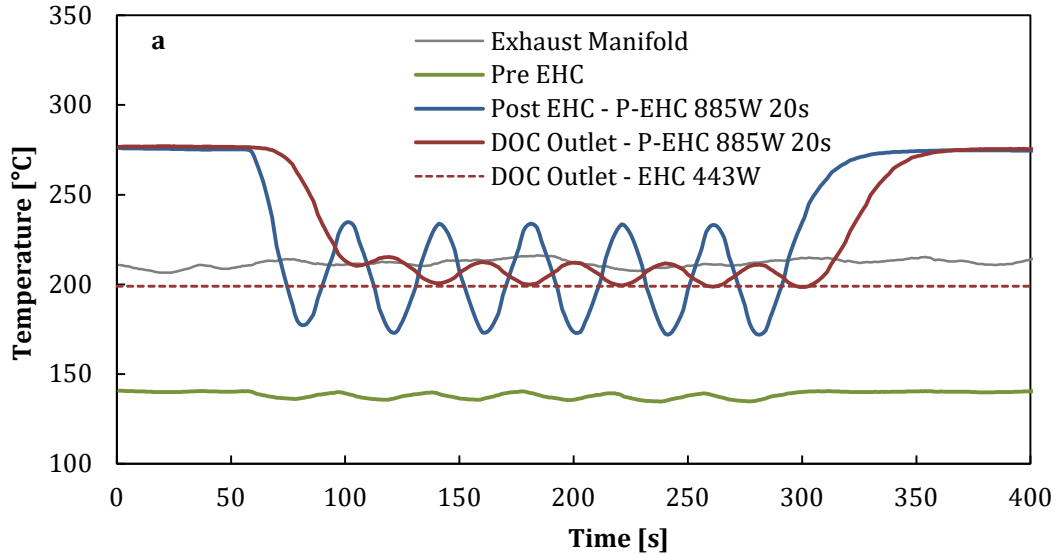
a
Exhaust Manifold
Pre EHC
Post EHC - P-EHC 885W 20s
DOC Outlet - P-EHC 885W 20s
DOC Outlet - EHC 443W
Temperature [°C]
Time [s]

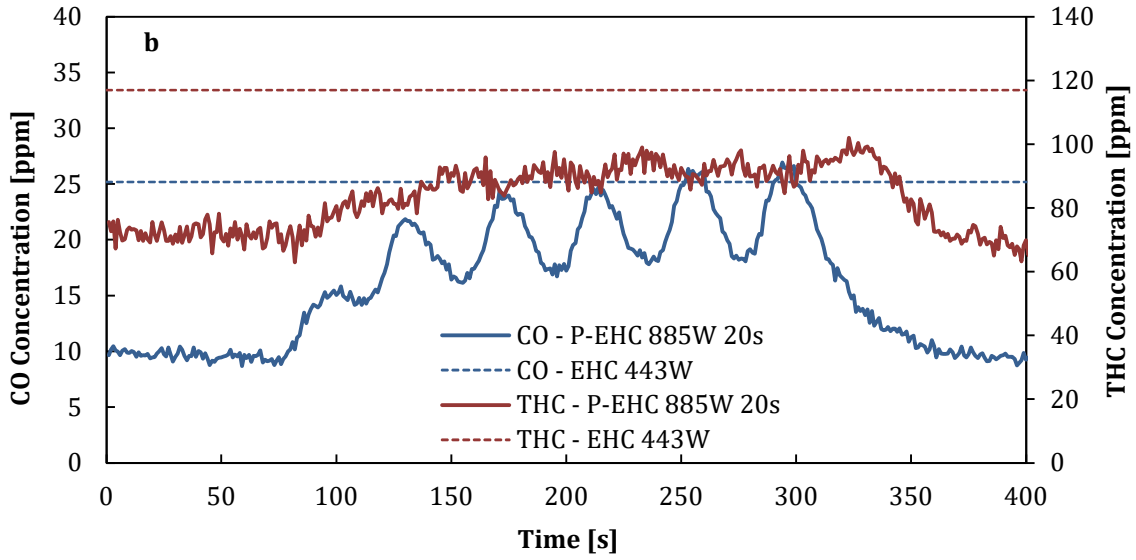
b
CO - P-EHC 885W 20s
CO - EHC 443W
THC - P-EHC 885W 20s
THC - EHC 443W
CO Concentration [ppm]
THC Concentration [ppm]
Time [s]

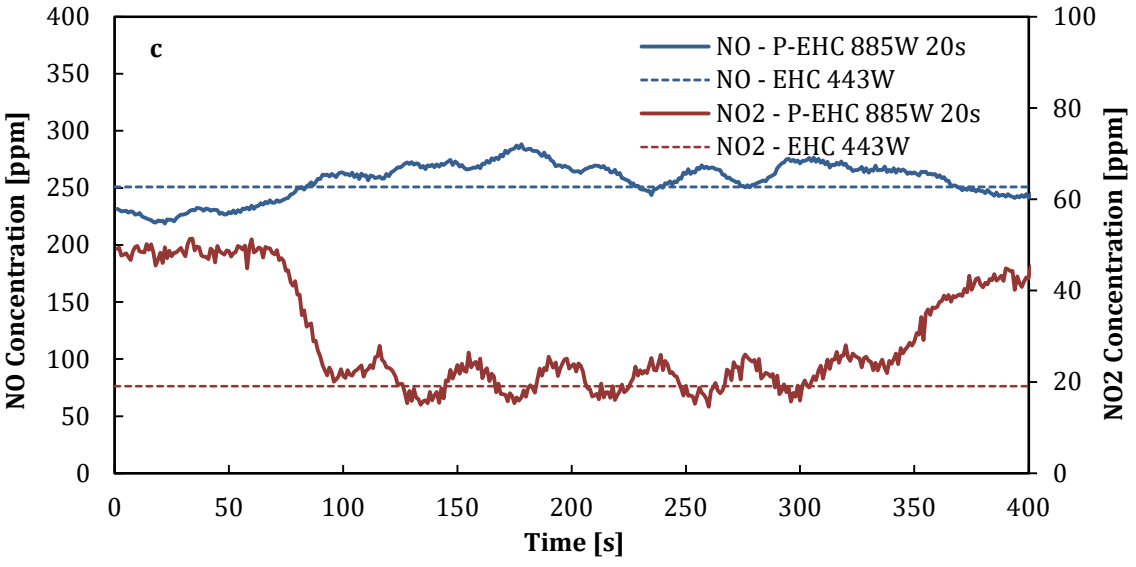
c
NO - P-EHC 885W 20s
NO - EHC 443W
NO2 - P-EHC 885W 20s
NO2 - EHC 443W
NO Concentration [ppm]
NO2 Concentration [ppm]
Time [s]

Figure 11: The Effect of Pulsating EHC on the a) DOC's Temperature Profiles, b) CO and THC Emissions at the DOC's Outlet, c) NO and NO_2 Emissions at the DOC's Outlet

The effect of the heating pulse width on the DOC's temperature profiles is shown in Figure 12. The 885 W of Pulsating heating with a pulse width of 10 seconds fluctuate the DOC's inlet temperature in the range of 197 °C to 205 °C. However, the DOC's outlet temperature remained stable at approximately 204 °C, which is 5 °C higher compared to steady electrical catalyst heating with similar electrical energy consumption. In this case, CO and THC emissions tended to reduce by approximately 13% and 18%, respectively, as shown in Figure 13. Results show that increasing the heating pulse width to 30 seconds can lead to extended temperature fluctuations at the DOC's inlet in the range of 154 °C to 255 °C.

Consequently, the DOC's outlet temperature varies from 183 °C to 228 °C over the pulsating heating period. Among the studied cases, the pulse width of 30 seconds showed the highest emissions reduction at the DOC's outlet with approximately 34% and 31% decrease in the CO and THC emissions, respectively. A further increase in the heating pulse width to 40 seconds leads to lower emissions' conversion performance. This can be attributed to the catalyst's light-out during the extended heating off period.

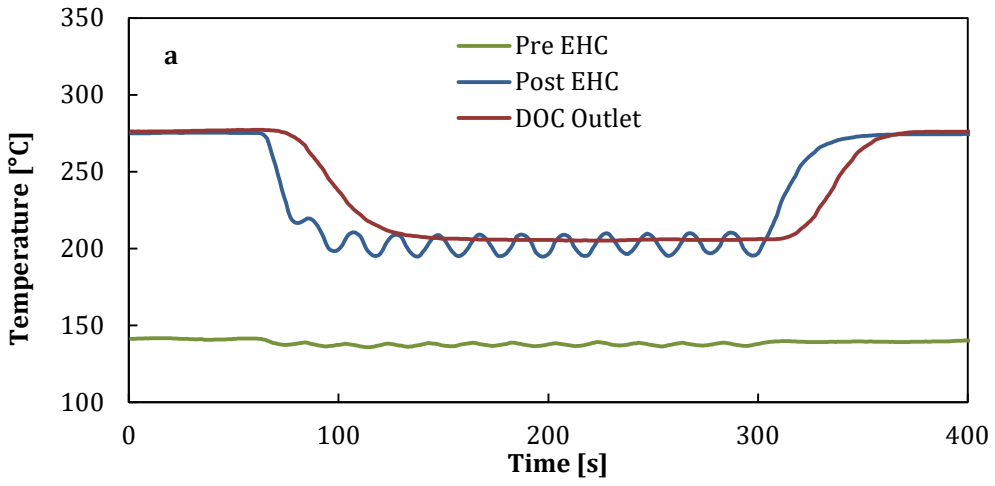

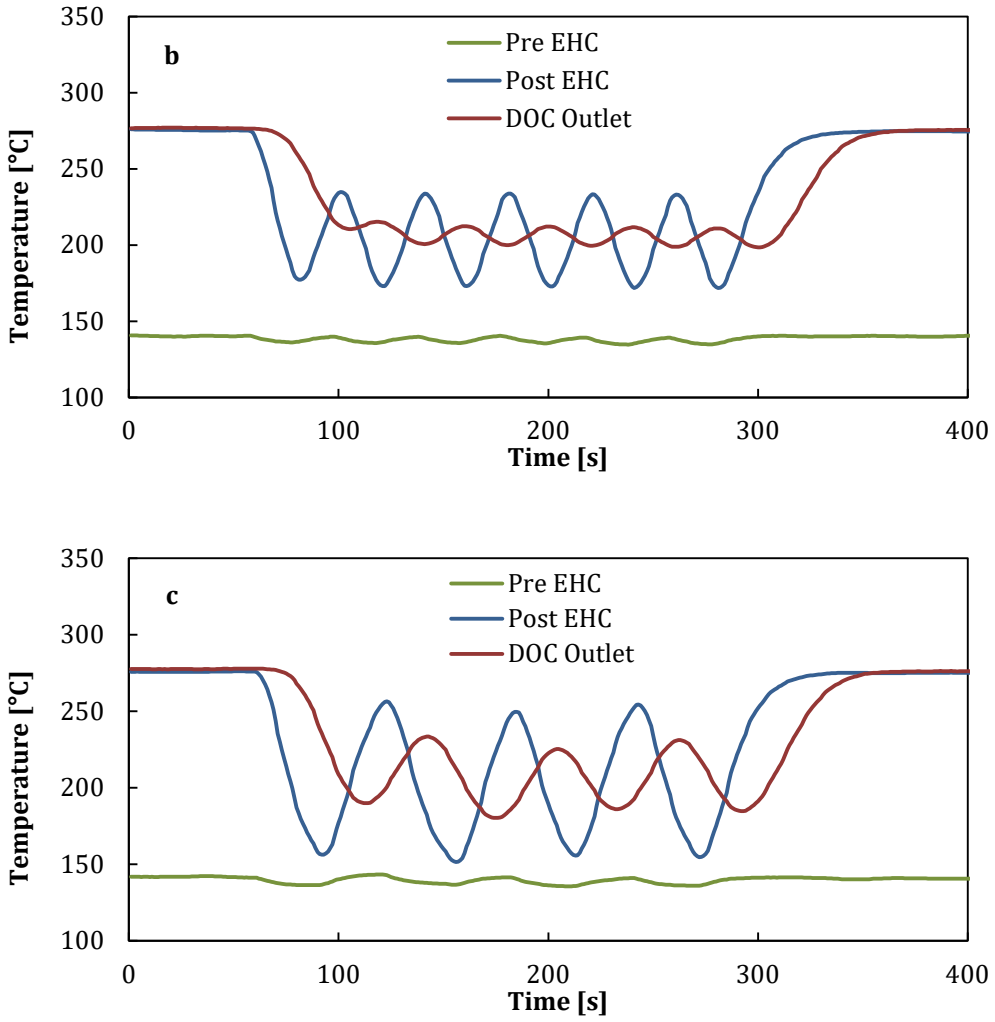

Figure 12: The Effect of 885 W P-EHC Pulse Width on the DOC's Temperature Profiles: a) Pulse Width: 10s, b) Pulse Width: 20s, c) Pulse Width: 30s

Considering the peaks in the DOC's inlet and outlet temperature profiles, it can be concluded that approximately 21 seconds are required for the heatwave to travel through the catalyst. In other words, the DOC's outlet temperature profile's phase is delayed by 21 seconds concerning the DOC's inlet temperature profile in these conditions. It should be noted that this parameter can be affected by other factors (e.g. catalyst geometry and exhaust flow rate).

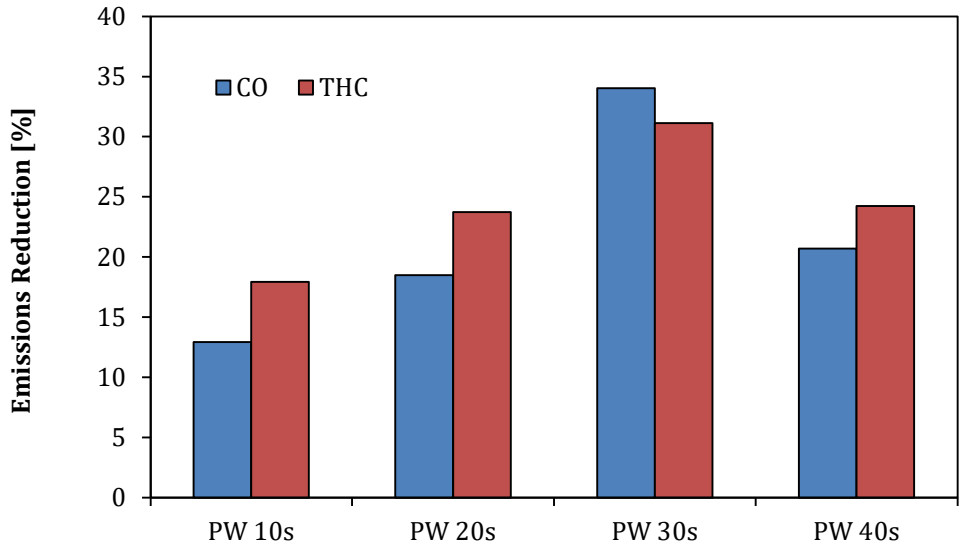

Figure 13: The Effect of Different P-EHC (885 W) Pulse Widths on the CO and THC Emissions' Reduction Compared to the EHC 443 W Case

Furthermore, computational investigation in Figure 14 shows that acceptable consistency was found for the model temperature profiles validation; however, the model tends to slightly overestimate the DOC's outlet temperature fluctuations. This can be associated with a higher heat loss in the experimental study.

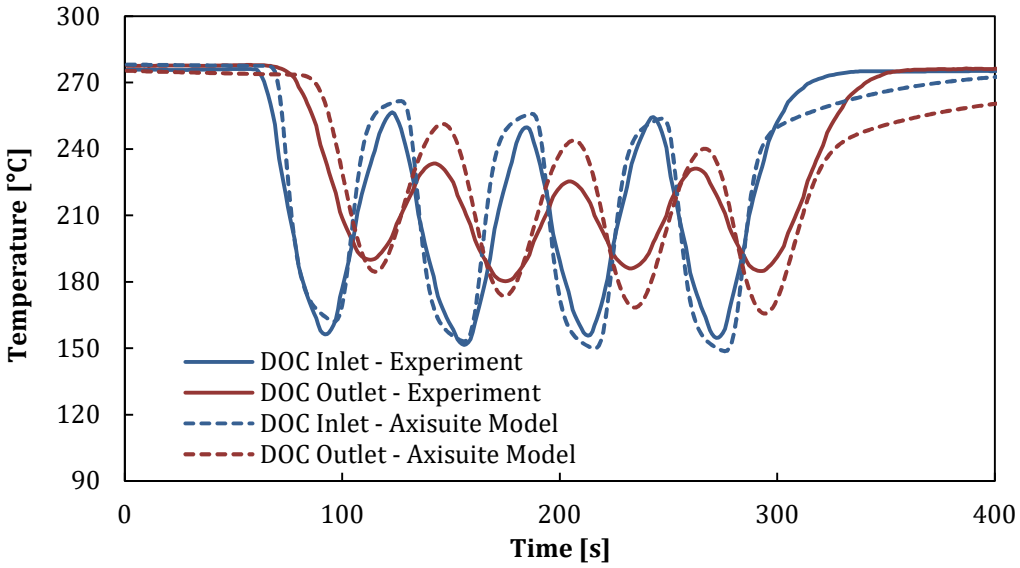

Figure 14: Calibration and Validation of the Axisuite Model based on the Experimental P-EHC Study (885 W Power and 30s Pulse Width)

Figure 15 demonstrates the DOC's temperature contours for different heating pulse widths during minimum and maximum temperature periods. Relatively homogenous temperature contours were observed in the case of the P-EHC with 10 seconds pulse width. The slight temperature fluctuations caused by the pulsating EHC at the catalyst's inlet tend to decrease considerably over the catalyst's length in this case. Results show that increasing the heating pulse width results in forming a hot spot with a higher temperature and larger size that travels through the catalyst. A cold spot follows this hot spot during the minimum temperature periods. For the case with 40 seconds heating pulse width, this cold spot can occupy the majority of the catalyst's volume and reduces the emissions' reduction performance. Therefore, this study reveals the importance of the heating control strategy in order to maximise the electrical catalyst heating efficiency on a driving cycle.

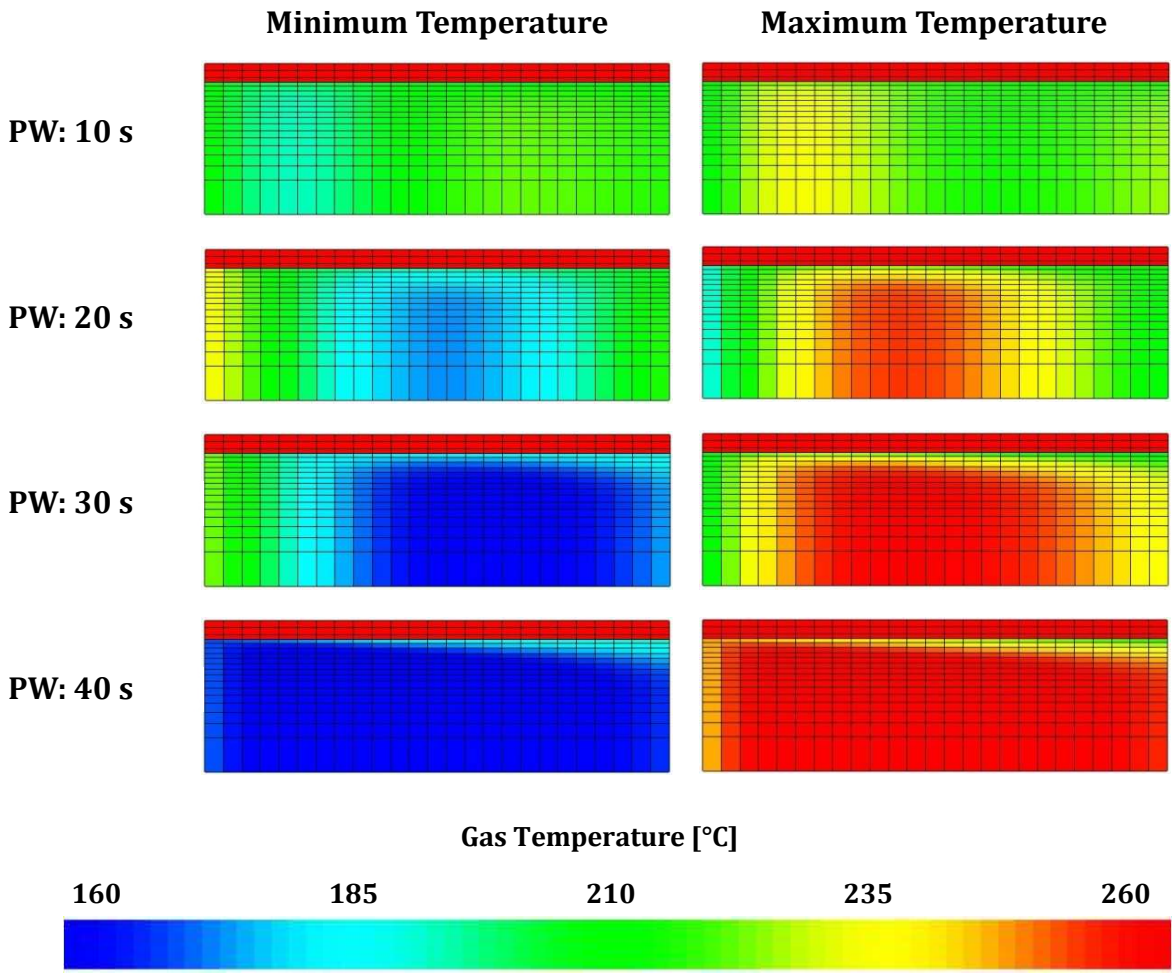

Figure 15: The Effect of Different P-EHC (885 W) Pulse Widths on the DOC's Temperature Contours

3.5. Fuel Post-injection for Catalyst Heating

As discussed previously, fuel post-injection can lead to higher heating efficiencies since the fuel can directly oxidise on the catalyst to produce heat. However, its effectiveness is highly dependent on the DOC's activity in oxidising the excessive hydrocarbon and CO emissions caused by the fuel post-injection. As listed in Table 3, fuel post-injection at 25° aTDC can increase the exhaust manifold's temperature by approximately 6 °C; this is mainly due to the late oxidation of the injected hydrocarbons in the relatively hot combustion chamber [34, 46]. This post-injection timing results in a 0.91% increase in the engine's ISFC compared to the reference case without

post-injection. Retarding the post-injection timing to 40° and 55° aTDC can considerably increase the ISFC by 2.48% and 3.25%. In these cases, post-injection contributes less to work generated by the engine, and a longer main injection is required to maintain the engine's load. The exhaust manifold's temperature slightly increases to approximately 218°C by retarding the post-injection from 25° aTDC to 40° aTDC and remains in a similar range in the 55° aTDC case. This can be attributed to higher fuel consumption and reduced engine's thermodynamic efficiency.

Table 3: Fuel Post-injection Effect on the Exhaust Manifold Temperature and ISFC

Case	Exhaust Manifold Temperature [°C]	ISFC [kg/kWh]	Change in the ISFC [%]
Post-injection Off - Ref	209.8	0.3199	-
Post-injection 25° aTDC	216.2	0.3228	0.91
Post-injection 40° aTDC	218.3	0.3228	2.48
Post-injection 55° aTDC	217.6	0.3303	3.25

As presented in Figure 16, retarding the post-injection timing can steadily increase the engine's CO emissions from 263 ppm in the 25° aTDC case to 342 ppm in the 55° aTDC case. This leads to similar behaviour in the DOC outlet CO concentrations while the catalyst's CO conversion efficiency slightly drops from 11% to 9.5%, 7.9% and 7%, respectively. Figure 16 shows that the engine's THC emissions are highly sensitive to the post-injection timing. The DOC's inlet THC emissions were increased from 273 ppm to 387 ppm by introducing the post-injection at 25° aTDC compared to the reference case. This was further increased to 603 ppm and 1390 ppm as the post-injection was retarded to 40° aTDC and 55° aTDC, respectively. Although a comparable amount of fuel was post-injected in these cases, delaying the post-injection timing can significantly affect the THC emissions. This is mainly caused by the drop in the combustion chamber's temperature that leads to lower oxidation of the post-injected fuel.

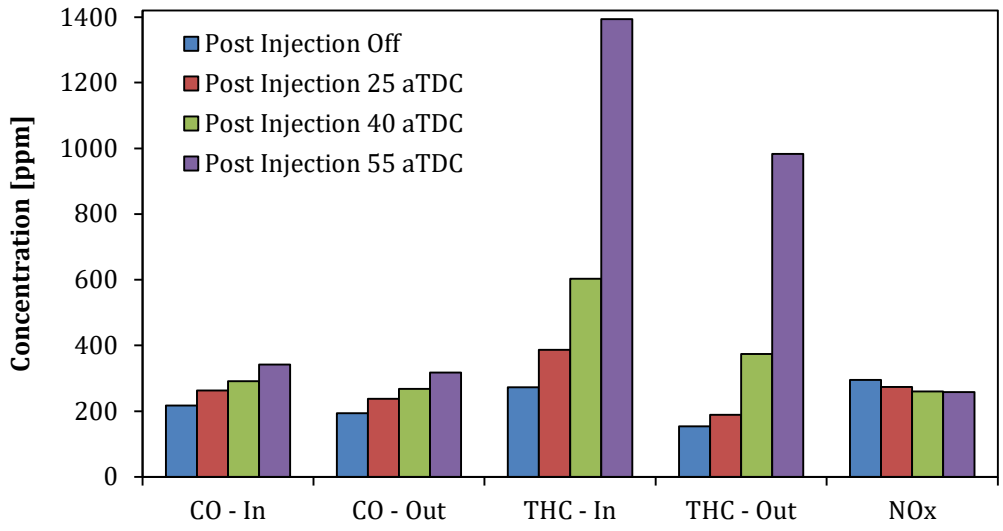

Figure 16: Fuel Post-injection Effect on the DOC's Inlet and Outlet Emissions Concentrations

The DOC's THC conversion efficiency tends to increase from 44% to 51% by applying the post-injection at 25° aTDC. However, delaying the post-injection shows a considerable reduction in the DOC's THC conversion efficiencies to 38% and 30% for the 40° aTDC and 55° aTDC cases, respectively. This can be associated with over-saturation of the DOC by excessive hydrocarbon emissions. On the other hand, a considerable decrease was observed in the engine's NO_x emissions by introducing the post-injection. The NO_x emissions were reduced by approximately 7% to 274 ppm by applying the post-injection at 25° aTDC compared to the reference case. Retarding the post-injection to 40° aTDC and 55° aTDC further reduced the NO_x emissions to approximately 260 ppm. This can be attributed to a reduced maximum in-cylinder temperature caused by the fuel post-injection [38, 39].

3.6. Combined EHC and Fuel Post-injection Catalyst Heating

In this section, 885 W of electrical heating in conjunction with fuel post-injection at different timing was investigated, as separately studied in previous sections. The combined heating strategy can benefit from the EHC's early catalyst light-off and the higher heating efficiency of the

fuel post-injection. Figure 17a shows that introducing the post-injection can roughly increase the post EHC's temperature by 3 °C when 885 W of electrical heating was applied. Results indicate that retarding the post-injection can considerably increase the DOC's outlet temperature. Comparing the post-injection at 55° aTDC case with the reference case without post-injection, a 21°C increase in the DOC's outlet temperature was observed. This was mainly caused by exothermic oxidation of the extra THC and CO emissions. Also, the CO concentrations at the DOC's outlet slightly increased by introducing and delaying the fuel post-injection, while the CO conversion efficiency remains at approximately 95% for the studied cases. As discussed in the previous section, the NO_x emissions tend to slightly reduce by introducing and delaying the fuel post-injection. A decrease in the NO_2 level was observed when the post-injection was applied. This can be attributed to: (i) the consumption of NO_2 in the oxidation reactions of THC and CO; (ii) reduced oxidation of NO to NO_2 due to inhibition of the DOC's active sites by excessive CO and HC emissions [47]. The THC concentrations at the DOC's outlet tend to significantly increase from 124 ppm to 296 ppm by retarding the post-injection from 25° aTDC to 55° aTDC, respectively. The results also indicate that the THC conversion efficiency increases from 68% to 79% by delaying the post-injection timing from 25° aTDC to 55° aTDC, respectively.

Combined electrical and fuel post-injection catalyst heating showed a significant improvement in the DOC's emissions conversion performance compared to the post-injection strategy. Although this approach can result in higher catalyst heating efficiencies leads to lower THC emissions which can be critical to meet the emissions legislations. Considering the increase in the DOC's outlet temperature, the combined heating strategy can be also beneficial for downstream aftertreatment component heating, e.g. DPF regeneration and SCR light-off.

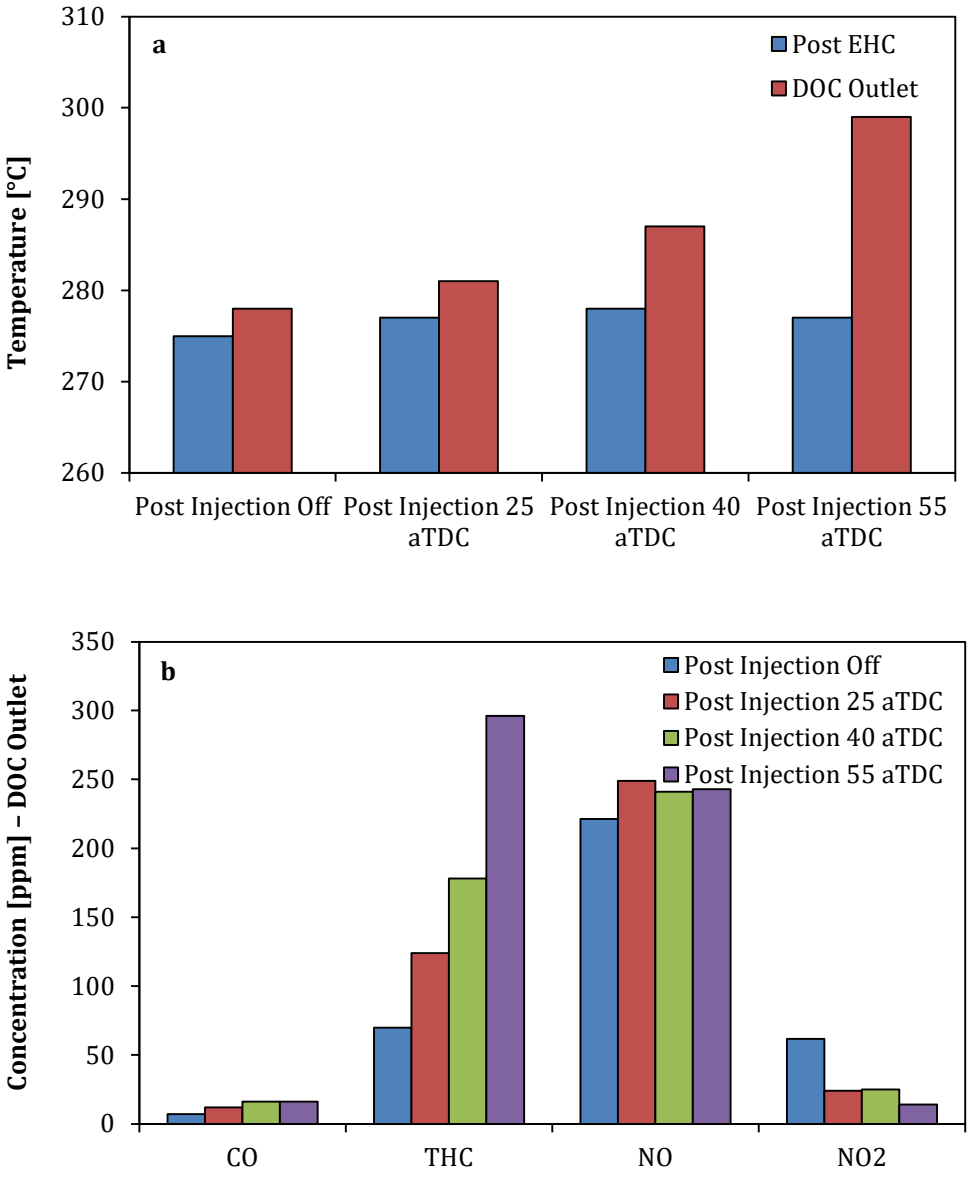

Figure 17: Combined EHC 885W and Fuel Post-injection Effect on the a) Aftertreatment System's Temperatures, b) the DOC's Outlet Emissions Concentrations

4. Conclusion

In this paper, active heating of diesel exhaust gas aftertreatment was investigated experimentally and computationally. The novel energy-efficient EHC control strategy was designed, investigated and optimised based on a diesel vehicle's aftertreatment requirement. This system, with a high potential to use in hybrid vehicles, showed excellent catalyst performance in the light-off time and gaseous emissions reduction.

Placing the electrical heating of the exhaust gas upstream of the catalyst can considerably increase the emissions' reduction performance compared to catalyst substrate and skin heating. Preliminary investigations in the Axisuite® model showed that electrical heating during 30 to 50 seconds of the NEDC reduces the cumulative CO and THC up to 47.2% and 17.8%, respectively. In this period, the thermal energy is more able to accelerate the catalyst's light-off with maintaining the oxidation reactions in the DOC. In the NEDC, 290 seconds after the cold-start, DOC outlet temperature decreases to 129 °C, which can light-out the catalyst. Hence, a two-phase electrical heating strategy prevents the catalyst from light-out (start at 20 seconds after the cold-start and lasts for 40 seconds, then starts at 210 seconds and lasts for 2- seconds). This novel strategy leads to approximate a 70% and 24% reduction in the cumulative CO and THC emissions, respectively.

Importantly, a novel pulsating EHC (P-EHC) control strategy was developed and evaluated to increase the electrical heating efficiency. It was experimentally found that 885 W of P-EHC with a pulse width of 30 seconds can considerably reduce the DOC's outlet CO and THC emissions (34% and 31%, respectively) when compared to steady EHC with similar electrical energy consumption. Further investigations revealed that P-EHC generates periodic hot spots at the DOC's inlet that can oxidise the CO and THC emissions. This increases the hot spot temperature as it travels through the catalyst by the exhaust gas flow. However, increasing the heating pulse width can light-out the catalyst between pulses and reduce the emissions' conversion performance.

Lastly, the combined heating and fuel post-injection strategy showed a substantial increase in the DOC's outlet temperature, which can be beneficial for DPF regeneration and SCR heating. Also, this strategy resulted in a significant reduction in THC emissions up to 79% compared to the post-injection strategy alone.

Acknowledgement

Jaguar Land Rover and the University of Birmingham are gratefully acknowledged for a financial grant to Mohammad Reza Hamedi. Jaguar Land Rover is also acknowledged for providing the funding for technical support.

Reference

[1] Davies C, Thompson K, Cooper A, Golunski S, Taylor SH, Bogarra Macias M, Doustdar O, Tsolakis A. Simultaneous Removal of NOx and Soot Particulate from Diesel Exhaust by In-situ Catalytic Generation and Utilisation of N2O. Applied Catalysis B: Environmental. 2018;239:10-5.

[2] Guille des Buttes A, Jeanneret B, Kéromnès A, Le Moyne L, Pélissier S. Energy management strategy to reduce pollutant emissions during the catalyst light-off of parallel hybrid vehicles. Applied Energy. 2020;266:114866.

[3] Serrano JR, Novella R, Piqueras P. Why the Development of Internal Combustion Engines Is Still Necessary to Fight against Global Climate Change from the Perspective of Transportation. Applied Sciences. 2019;9(21):4597.

[4] Lion S, Vlaskos I, Taccani R. A review of emissions reduction technologies for low and medium speed marine Diesel engines and their potential for waste heat recovery. Energy Conversion and Management. 2020;207:112553.

[5] Leach F, Kalghatgi G, Stone R, Miles P. The scope for improving the efficiency and environmental impact of internal combustion engines. Transportation Engineering. 2020;1:100005.

[6] Boutikos P, Žák A, Kočí P. CO and hydrocarbon light-off inhibition by pre-adsorbed NOx on Pt/CeO2/Al2O3 and Pd/CeO2/Al2O3 diesel oxidation catalysts. Chemical Engineering Science. 2019;209:115201.

[7] Zhang Y, Lou D, Tan P, Hu Z. Experimental study on the durability of biodiesel-powered engine equipped with a diesel oxidation catalyst and a selective catalytic reduction system. Energy. 2018;159:1024-34.

[8] Kim B-S, Jeong H, Bae J, Kim PS, Kim CH, Lee H. Lean NOx trap catalysts with high low-temperature activity and hydrothermal stability. Applied Catalysis B: Environmental. 2020;270:118871.

[9] Caliskan H, Mori K. Environmental, enviroeconomic and enhanced thermodynamic analyses of a diesel engine with diesel oxidation catalyst (DOC) and diesel particulate filter (DPF) after treatment systems. Energy. 2017;128:128-44.

[10] Hamedi MR, Doustdar O, Tsolakis A, Hartland J. Thermal energy storage system for efficient diesel exhaust aftertreatment at low temperatures. Applied Energy. 2019;235:874-87.

[11] Zeng Y, Cai Y, Chu C, Kou G, Gao W. Integrated Energy and Catalyst Thermal Management for Plug-In Hybrid Electric Vehicles. Energies. 2018;11(7):1761.

[12] Xiong H, Wiebenga MH, Carrillo C, Gaudet JR, Pham HN, Kunwar D, Oh SH, Qi G, Kim CH, Datye AK. Design considerations for low-temperature hydrocarbon oxidation reactions on Pd based catalysts. Applied Catalysis B: Environmental. 2018;236:436-44.

[13] Konagai N, Takeshita T, Azuma N, Ueno A. Preparation of Fe−Cr Wires with Dispersed Co3O4 as an Electrically Heated Catalyst for Cold-Start Emissions. Industrial & Engineering Chemistry Research. 2006;45(9):2967-72.

[14] Gao J, Tian G, Sorniotti A, Karci AE, Di Palo R. Review of thermal management of catalytic converters to decrease engine emissions during cold start and warm up. Applied Thermal Engineering. 2019;147:177-87.

[15] Gong C, Huang K, Deng B, Liu X. Catalyst light-off behavior of a spark-ignition LPG (liquefied petroleum gas) engine during cold start. Energy. 2011;36(1):53-9.

[16] Deng Y, Liu H, Zhao X, E J, Chen J. Effects of cold start control strategy on cold start performance of the diesel engine based on a comprehensive preheat diesel engine model. Applied Energy. 2018;210:279-87.

[17] Park S, Woo S, Shon J, Lee K. Experimental study on heat storage system using phase-change material in a diesel engine. Energy. 2017;119:1108-18.

[18] Piqueras P, García A, Monsalve-Serrano J, Ruiz MJ. Performance of a diesel oxidation catalyst under diesel-gasoline reactivity controlled compression ignition combustion conditions. Energy Conversion and Management. 2019;196:18-31.

[19] Lefort I, Herreros JM, Tsolakis A. Reduction of Low Temperature Engine Pollutants by Understanding the Exhaust Species Interactions in a Diesel Oxidation Catalyst. Environmental Science & Technology. 2014;48(4):2361-7.

[20] Ramanathan; Karthik OSH, Bissett; Edward J. . Electrically Heated Catalysts for Hybrid Applications: Mathematical Modeling and Analysis. Industrial & Engineering Chemistry Research. 2011;50(14):8444-67.

[21] Presti M, Pace L, Poggio L, Rossi V. Cold Start Thermal Management with Electrically Heated Catalyst: A Way to Lower Fuel Consumption. SAE International 2013-24-0158; 2013, https://doi.org/10.4271/2013-24-0158

[22] Culbertson D, Khair M, Zhang S, Tan J, Spooler J. The Study of Exhaust Heating to Improve SCR Cold Start Performance. SAE Int. J. Engines; 2015. https://doi.org/10.4271/2015-01-1027

[23] Maus W, Brück R, Konieczny R, Scheeder A. Electrically heated catalyst for thermal management in modern vehicle applications. MTZ worldwide. 2010;71(5):34-9.

[24] Pfahl U, Schatz A, Konieczny R. Advanced Exhaust Gas Thermal Management for Lowest Tailpipe Emissions - Combining Low Emission Engine and Electrically Heated Catalyst. SAE International 2012-01-1090; 2012, https://doi.org/10.4271/2012-01-1090

[25] Thomas Knorr DE, Oliver Maiwald, Axel Schatz, Rolf Brück The Electric Heatable Catalyst – An Efficient Measure for Emission Optimization in Mild Hybrid Vehicle Operation Strategies. 24th Aachen Colloquium Automobile and Engine Technology 2015 2015,

[26] Pace L, Presti M. An Alternative Way to Reduce Fuel Consumption During Cold Start: The Electrically Heated Catalyst. SAE International 2011-24-0178. 2011, https://doi.org/10.4271/2011-24-0178

[27] Horng R-F, Chou H-M, Hsu T-C. Reaction of the electrically-heated catalyst of a four-stroke motorcycle engine under cold-start conditions with additional enrichment of the intake mixture. Proceedings of the Institution of Mechanical Engineers, Part D: Journal of Automobile Engineering. 2003;217(12):1117-24.

[28] Socha LS, Thompson DF. Electrically Heated Extruded Metal Converters for Low Emission Vehicles. SAE International 920093; 1992, https://doi.org/10.4271/920093

[29] Massaguer A, Pujol T, Comamala M, Massaguer E. Feasibility study on a vehicular thermoelectric generator coupled to an exhaust gas heater to improve aftertreatment's efficiency in cold-starts. Applied Thermal Engineering. 2020;167:114702.

[30] Zobel T, Schürch C, Boulouchos K, Onder C. Reduction of Cold-Start Emissions for a Micro Combined Heat and Power Plant. Energies. 2020;13(8):1862.

[31] Gao J, Tian G, Sorniotti A. On the emission reduction through the application of an electrically heated catalyst to a diesel vehicle. Energy Science & Engineering. 2019;7(6):2383-97.

[32] Kim CH, Paratore M, Gonze E, Solbrig C, Smith S. Electrically Heated Catalysts for Cold-Start Emissions in Diesel Aftertreatment. SAE International 2012-01-1092; 2012, https://doi.org/10.4271/2012-01-1092

[33] Farhan SM, Pan W, Yan W, Jing Y, Lili L. Impact of post-injection strategies on combustion and unregulated emissions during different loads in an HSDI diesel engine. Fuel. 2020;267:117256.

[34] Merola SS, De Filippo A, Valentino G, Tornatore C, Marchitto L, Iannuzzi S. Optical Investigation of Post-injection Strategy Impact on the Fuel Vapor within the Exhaust Line of a Light Duty Diesel Engine Supplied with Biodiesel Blends. SAE International 2013-01-1127; 2013, https://doi.org/10.4271/2013-01-1127

[35] O'Connor J, Musculus M. Post Injections for Soot Reduction in Diesel Engines: A Review of Current Understanding. SAE Int. J. Engines 6 (1); 2013. https://doi.org/10.4271/2013-01-0917

[36] Yun H, Reitz RD. An Experimental Investigation on the Effect of Post-Injection Strategies on Combustion and Emissions in the Low-Temperature Diesel Combustion Regime. Journal of Engineering for Gas Turbines and Power. 2005;129(1):279-86.

[37] Arrègle J, Pastor JV, López JJ, García A. Insights on postinjection-associated soot emissions in direct injection diesel engines. Combustion and Flame. 2008;154(3):448-61.

[38] Desantes JM, Arrègle J, López JJ, García A. A Comprehensive Study of Diesel Combustion and Emissions with Post-injection. SAE International 2007-01-0915; 2007, https://doi.org/10.4271/2007-01-0915

[39] Poorghasemi K, Ommi F, Yaghmaei H, Namaki A. An investigation on effect of high pressure post injection on soot and NO emissions in a DI diesel engine. Journal of Mechanical Science and Technology. 2012;26(1):269-81.

[40] Payri F, Benajes J, Pastor JV, Molina S. Influence of the Post-Injection Pattern on Performance, Soot and NOx Emissions in a HD Diesel Engine. SAE International 2002-01-0502; 2002, https://doi.org/10.4271/2002-01-0502

[41] Yamamoto K, Takada K, Kusaka J, Kanno Y, Nagata M. Influence of Diesel Post Injection Timing on HC Emissions and Catalytic Oxidation Performance. SAE International 2006-01-3442; 2006, https://doi.org/10.4271/2006-01-3442

[42] Lafossas F, Matsuda Y, Mohammadi A, Morishima A, Inoue M, Kalogirou M, Koltsakis G, Samaras Z. Calibration and Validation of a Diesel Oxidation Catalyst Model: from Synthetic Gas Testing to Driving Cycle Applications. SAE International Journal of Engines. 2011;4(1):1586-606.

[43] Satterfield CN. Heterogeneous Catalysis in Practice. McGraw-Hill chemical engineering series: McGraw-Hill, 1980.

[44] Thomas JMT, W. John. Principles and Practice of Heterogeneous Catalysis: Wiley VCH, 2nd Edition, 2014.

[45] Horng R-F, Chou H-M. Effect of input energy on the emission of a motorcycle engine with an electrically heated catalyst in cold-start conditions. Applied Thermal Engineering. 2004;24(14):2017-28.

[46] Mohan B, Yang W, Chou Sk. Fuel injection strategies for performance improvement and emissions reduction in compression ignition engines—A review. Renewable and Sustainable Energy Reviews. 2013;28:664-76.

[47] Herreros JM, Gill SS, Lefort I, Tsolakis A, Millington P, Moss E. Enhancing the low temperature oxidation performance over a Pt and a Pt–Pd diesel oxidation catalyst. Applied Catalysis B: Environmental. 2014;147:835-41.